medRxiv preprint doi: https://doi.org/10.1101/2022.07.11.22277322; this version posted July 13, 2022. The copyright holder for this preprint (which was not certified by peer review) is the author/funder, who has granted medRxiv a license to display the preprint in perpetuity. All rights reserved. No reuse allowed without permission.

Spatiotemporal evolution of the ccRCC microenvironment links intra-tumoral heterogeneity to immune escape

Mahdi Golkaram,[1] Fengshen Kuo,[2] Sounak Gupta,[3] Maria I. Carlo,[4] Michael L. Salmans,[1] Raakhee Vijayaraghavan,[1] Cerise Tang,[5] Vlad Makarov,[2,5] Phillip Rappold,[5] Kyle A. Blum,[2,5,6] Chen Zhao,[1] Rami Mehio,[1] Shile Zhang,[1] Jim Godsey,[1] Traci Pawlowski,[1] Renzo G. DiNatale,[2,5,6] Luc GT Morris,[7] Jeremy Durack,[8] Paul Russo,[6] Ritesh R. Kotecha,[4] Jonathan Coleman,[6] Ying-Bei Chen,[3] Victor E Reuter,[3] Robert J Motzer,[4] Martin H. Voss,[4] Li Liu,[1,15,*] Ed Reznik,[6,9,10,15,*] Timothy A. Chan,[2,11,12,13,14,15,*] and A. Ari Hakimi[2,6,15,16,*]

[1]Illumina, Inc., 5200 Illumina Way, San Diego, CA 92122, USA

[2]Immunogenomics and Precision Oncology Platform, Memorial Sloan Kettering Cancer Center, New York, NY 10065, USA

[3]Department of Pathology, Memorial Sloan Kettering Cancer Center, New York, NY 10065, USA

[4]Department of Medicine, Genitourinary Oncology, Memorial Sloan Kettering Cancer Center, New York, New York, NY 10065, USA

[5]Human Oncology and Pathogenesis Program, Memorial Sloan Kettering Cancer Center, New York, NY 10065, USA

[6]Urology Service, Department of Surgery, Memorial Sloan Kettering Cancer Center, New York, NY 10065, USA

[7]Department of Surgery, Head & Neck Service, Memorial Sloan Kettering Cancer Center, New York, NY 10065, USA

[8]Interventional Radiology, Memorial Sloan Kettering Cancer Center, New York, NY 10065, USA

[9]Computational Oncology Service, Memorial Sloan Kettering Cancer Center, New York, NY, 10065, USA

[10]Marie-Josée and Henry R. Kravis Center for Molecular Oncology, Memorial Sloan Kettering Cancer Center, New York, NY, 10065, USA

[11]Department of Radiation Oncology, Memorial Sloan Kettering Cancer Center, New York, NY 10065, USA

[12]Center for Immunotherapy and Precision Immuno-Oncology, Cleveland Clinic, Cleveland, OH 44195, USA

[13]Lerner Research Institute, Cleveland Clinic, Cleveland, OH 44195, USA

[14]National Center for Regenerative Medicine, Cleveland Clinic, Cleveland, OH 44195, USA

[15]Senior author

[16]Lead contact

*Correspondence: reznike@mskcc.org, (E.R.), lliu3@illumina.com (L.L), chant2@ccf.org (T.A.C.), hakimia@mskcc.org (A.A.H).

medRxiv preprint doi: https://doi.org/10.1101/2022.07.11.22277322; this version posted July 13, 2022. The copyright holder for this preprint (which was not certified by peer review) is the author/funder, who has granted medRxiv a license to display the preprint in perpetuity. All rights reserved. No reuse allowed without permission.

Abstract

Background

Intratumoral heterogeneity (ITH) is a hallmark of clear cell renal cell carcinoma (ccRCC) that reflects the trajectory of evolution and influences clinical prognosis. Here we seek to elucidate how ITH and tumor evolution during immune checkpoint inhibitor (ICI) treatment can lead to therapy resistance.

Methods

Here, we spatiotemporally profiled the genomic and immunophenotypic characteristics of 29 ccRCC patients, including pre- and post-therapy samples from 17 ICI treated patients.

Deep multi-regional whole exome and transcriptome sequencing were performed on 29 patients at different time points before and after ICI therapy. T cell repertoire was also monitored from tissue and peripheral blood collected from a subset of patients to study T cell clonal expansion during ICI therapy.

Results

Angiogenesis, lymphocytic infiltration, and myeloid infiltration varied significantly across regions of the same patient, potentially confounding their utility as biomarkers of ICI response. Elevated ITH associated with a constellation of both genomic features (HLA LOH, CDKN2A/B loss) and microenvironmental features, including elevated myeloid expression, reduced peripheral T cell receptor (TCR) diversity, and putative neoantigen depletion. Hypothesizing that ITH may itself play a role in shaping ICI response, we derived a transcriptomic signature associated with

medRxiv preprint doi: https://doi.org/10.1101/2022.07.11.22277322; this version posted July 13, 2022. The copyright holder for this preprint (which was not certified by peer review) is the author/funder, who has granted medRxiv a license to display the preprint in perpetuity. All rights reserved. No reuse allowed without permission.

neoantigen depletion that strongly associated with response to ICI and targeted therapy treatment in several independent clinical trial cohorts.

Conclusions

These results argue that genetic and immune heterogeneity jointly co-evolve and influence response to ICI in ccRCC.

Trial registration

We completed a single-arm pilot study at Memorial Sloan Kettering Cancer Center (MSKCC; ClinicalTrials.gov identifier NCT02595918) to examine the safety and feasibility of neoadjuvant nivolumab in patients with localized RCC.

Background

Clear cell renal cell carcinoma (ccRCC) is the most common histological subtype of kidney cancer and demonstrates a high response rate to immune checkpoint inhibitors such as nivolumab, pembrolizumab and ipilimumab [1-3]. However, only a subset of ccRCC patients respond to ICI, and biomarkers for ICI response in other disease settings such as tumor mutation burden, neoantigen load and mismatch repair deficiency do not associate with ICI response in ccRCC [4-7]. Recently, several studies have identified transcriptomic microenvironmental features including angiogenic gene expression, T-cell infiltration, and myeloid activation that correlate with response or resistance to ICI and combination therapies in ccRCC [7-13]. This suggests that the ccRCC microenvironment, in addition to genomic factors, influences ICI response.

medRxiv preprint doi: https://doi.org/10.1101/2022.07.11.22277322; this version posted July 13, 2022. The copyright holder for this preprint (which was not certified by peer review) is the author/funder, who has granted medRxiv a license to display the preprint in perpetuity. All rights reserved. No reuse allowed without permission.

In parallel, recent work has demonstrated the prevalence of ITH in untreated ccRCC [14]. This study has largely focused on heterogeneity in the presence of key driver mutations and copy number alterations and have demonstrated that ccRCC tumors follow one of a small number of evolutionary trajectories, each of which are associated with distinct patterns of genomic ITH and clinical prognosis. However, the potential for non-genomic heterogeneity in the tumor microenvironment, including but not limited to variability in the amount and identity of immune cells in spatially distinct regions of the same tumor is overlooked. Recently, we and others described substantial heterogeneity in the tumor-microenvironment (TME) in several small cohorts of ccRCC tumors both in the treatment-naïve and treatment-exposed settings, raising the possibility that heterogeneity in the TME may itself shape the evolution of the tumor and its likelihood to respond to therapy [15, 16].

In this study, we hypothesized ccRCC tumors with elevated ITH constitute a genomically and immunologically distinct class of tumors, with distinguishing clonal/subclonal genomic alterations, immunologic profiles, and therapeutic response trajectories. To test this hypothesis, we utilize whole exome sequencing (WES), whole transcriptome sequencing (WTS), TCRseq, and histopathologic multi-regional data across a cohort of untreated and ICI exposed patients from a phase 2 clinical trial to reveal the molecular determinants of therapy response in ccRCC (Fig. 1 and Table S1). Our integrated analysis demonstrated that ITH is highly correlated among genomic, transcriptomic, and TME characteristics. ITH-high tumors are enriched for features including SETD2 and PBRM1 mutations, HLA loss of heterozygosity (HLA LOH), and CDKN2A/B loss. Immunologically, ITH-high tumors display a depletion of putative neoantigens, elevated myeloid activation, and reduced T cell diversity, that are in aggregate associated with escape from the anti-tumor immune response. Premised on these observations, we developed a

medRxiv preprint doi: https://doi.org/10.1101/2022.07.11.22277322; this version posted July 13, 2022. The copyright holder for this preprint (which was not certified by peer review) is the author/funder, who has granted medRxiv a license to display the preprint in perpetuity. All rights reserved. No reuse allowed without permission.

transcriptional signature for immune escape which correlates with distinct histopathologic patterns and is associated with ICI resistance across several diverse clinical trial cohorts.

Materials and Methods

Sample acquisition

After acquiring informed consent and institutional review board approval from Memorial Sloan Kettering Cancer Center (MSK), partial or radical nephrectomies were performed at MSK (New York) and stored at the MSK Translational Kidney Research Program (TKRCP). Samples were flash frozen and stored at -80 degrees Celsius prior to molecular characterization. Clinical metadata was recorded for all tumor samples. All patients represent clear cell histology and were treated via ICI alone or in combination with tyrosine kinase inhibitor (TKI). All treatments were administered prior to surgery in a neo-adjuvant setting and biopsies were collected. Detailed clinical data and treatment regimen for each patient is included in Table S2.

Untreated cohort

Using and institutional database we identified six patients with advanced or metastatic ccRCC that underwent nephrectomy with multiregional data available MR01,02,03,05,06, SC03. Clinical and pathologic data is available in Table S2.

Neoadjuvant multiregional cohort

This open-label, single-arm, pilot study was done at Memorial Sloan Kettering Cancer Center and funded through the National Institute of Health's Cancer Therapy Evaluation Program (CTEP). Patients received nivolumab (dose initially 3 mg/kg, then protocol amended to 240 mg

medRxiv preprint doi: https://doi.org/10.1101/2022.07.11.22277322; this version posted July 13, 2022. The copyright holder for this preprint (which was not certified by peer review) is the author/funder, who has granted medRxiv a license to display the preprint in perpetuity. All rights reserved. No reuse allowed without permission.

flat dose) every 2 weeks for 4 treatments. Surgery was planned 7-14 days after the last dose. Prior to starting therapy, all patients had a kidney biopsy to confirm ccRCC, and tumor staging with renal protocol MRI and CT of the chest. After 4 doses and prior to surgery, patients also had a renal protocol MRI. Changes in primary tumor size were assessed according to Response Evaluation Criteria in Solid Tumors (RECIST) version 1.1. Resection of the primary tumor and lymph nodes was done according to standard institutional procedures. From May 27, 2016, to September 9, 2019, 21 patients were screened and 18 were enrolled into the study of which 17 had available genomic data. Baseline patient characteristics are in Supplementary Table S2. All patients had localized disease at time of enrollment and biopsy-proven clear cell RCC. Perioperative and pathological details are included in Supplementary Table S2. Median time to nephrectomy after the last dose of nivolumab was 10.5 days (range, 9-13 days).

Metastatic multiregional Cohort

Using an institutional database, we identified 6 additional patients who had received ICI prior to nephrectomy (Supplementary Table S2). All patients had metastatic disease at time of ICI; two received anti-VEGF therapies before ICI.

Multi-regional sampling

For the prospective neoadjuvant trial and the “MR” samples single region biopsies were obtained preoperatively. Following nephrectomy, tumor were bivalved and 5 regions were chosen: One region from the tumor center and 4 from each quadrant (upper medial, upper later, lower medial, lower lateral). Grossly necrotic or hemorrhagic regions were avoided. For the remaining samples (those treated with definitive immunotherapy “SC”) regions were taken from distinct regions of tumors separated by 1-2 cm avoiding grossly necrotic or hemorrhagic regions).

medRxiv preprint doi: https://doi.org/10.1101/2022.07.11.22277322; this version posted July 13, 2022. The copyright holder for this preprint (which was not certified by peer review) is the author/funder, who has granted medRxiv a license to display the preprint in perpetuity. All rights reserved. No reuse allowed without permission.

143

144 **Whole exome sequencing**

145 Libraries for whole exome sequencing were generated with TruSight Oncology DNA
146 Library Prep Kit with 40ng input DNA per sample. TruSight Oncology index PCR products were
147 directly used for enrichment and target exome enrichment was performed using the IDT xGen
148 Universal Blockers and IDT xGen Exome Research panel. A single-plex hybridization was done
149 overnight at 65°C. Accuclear dsDNA Ultra High Sensitivity assay (Biotium) was used for library
150 quantification of the post-enriched libraries. Post enrichment libraries were normalized using
151 bead-based normalization and pooled. Samples were sequenced with 101 bp paired-end reads
152 on Illumina NovaSeq™ 6000 S4 flow cell using the XP workflow for individual lane loading (12-
153 plex per lane). On average, each sample yielded 500 million reads and
154 MEDIAN_TARGET_COVERAGE depth of 360X.

155

156 **Whole transcriptome sequencing**

157 Libraries for whole transcriptome RNA-seq were generated with Illumina TruSeq Stranded
158 Total RNA. 100 ng RNA was used as input for Ribo-Zero rRNA Removal Kit, with Illumina TruSeq
159 RNA UD Indexes (96 indexes) for sample indexing. Qubit dsDNA High Sensitivity assay (Thermo
160 Fisher Scientific) was used for library quantification. Sequencing was done on Illumina
161 NovaSeq™ 6000 S2 (36-plex) or S4 (72-plex) flow cell with 76 bp paired-end sequencing to
162 produce ~200 million paired reads per library.

163

164 **T-cell repertoire sequencing**

medRxiv preprint doi: https://doi.org/10.1101/2022.07.11.22277322; this version posted July 13, 2022. The copyright holder for this preprint (which was not certified by peer review) is the author/funder, who has granted medRxiv a license to display the preprint in perpetuity. All rights reserved. No reuse allowed without permission.

Libraries for T-cell repertoire sequencing were generated with AmpliSeq for Illumina Library PLUS paired with AmpliSeq cDNA Synthesis for Illumina with 100 ng RNA input per cDNA synthesis reaction. The TCR beta-SR Panel was used for generating amplicons, and AmpliSeq CD Indexes Set A for Illumina were used for sample barcodes. Qubit dsDNA High Sensitivity assay (Thermo Fisher Scientific) was used for library quantification. Sequencing was done on the NextSeq 550 (41-plex) with 151 bp paired-end sequencing to produce ~5 million paired reads per library.

WTS pipeline

WTS raw read sequences were aligned against human genome assembly hg19 by STAR 2-pass alignment [17]. QC metrics, for example general sequencing statistics, gene feature and body coverage, were then calculated based on the alignment result through RSeQC. WTS gene level count values were computed by using the R package GenomicAlignments [18] over aligned reads with UCSC KnownGene [19] in hg19 as the base gene model. The union counting mode was used and only mapped paired reads after alignment quality filtering were considered. Finally, gene level FPKM (Fragments Per Kilobase Million) and raw read count values were computed by the R package DESeq2 [20].

ESTIMATE

The ESTIMATEScore, which is the estimate of the presence of stromal and immune cells in tumor tissue, is calculated through the ESTIMATE R package [21] based on a given gene expression profile in FPKM.

medRxiv preprint doi: https://doi.org/10.1101/2022.07.11.22277322; this version posted July 13, 2022. The copyright holder for this preprint (which was not certified by peer review) is the author/funder, who has granted medRxiv a license to display the preprint in perpetuity. All rights reserved. No reuse allowed without permission.

188 **Immune deconvolution analysis**

189 Two distinct popular computational methods, ssGSEA [22] and CIBERSORT [23], were
190 chosen for immune deconvolution analysis. Signature gene lists of immune cell types for ssGSEA
191 were obtained from Bindea et al. [24] and Senbabaoglu et al. [3]. ssGSEA takes the sample FPKM
192 WTS expression values as the input and computes an enrichment score for the given gene list of
193 immune cell type relative to all other genes in the transcriptome. On the other hand, CIBERSORT
194 also takes FPKM WTS expression values as the input but uses a signature gene expression
195 matrix of interest immune cell types instead to compute the infiltration level of each immune cell
196 type. The LM22 immune cell signature which was validated and published along with
197 CIBERSORT is used. We also used FRICTION [25] to deconvolute WTS into absolute CD8 and
198 CD4 T cells as well as CD19 B cells.

199

200 **HERV quantification**

201 We used WTS to quantify HERVs as described before [25]. Briefly, all WTS reads were
202 aligned (using STAR aligner with optimized multi mapping options) to a custom genome built were
203 human reference (hg19) and HERV specific reference are combined. Then reads aligned to non-
204 HERV genes are removed and the rest are annotated. 3 samples contained super high median
205 HERVs (Grubbs test $P<0.05$) and removed for better visualization.

206

207 **WES analysis pipeline**

208 Raw sequencing data were aligned to the hg19 genome build using the Burrows-Wheeler
209 Aligner (BWA) version 0.7.17 [26]. Further indel realignment, base-quality score recalibration and
210 duplicate-read removal were performed using the Genome Analysis Toolkit (GATK) version 3.8
211 [27] following raw reads alignments guidelines [28]. VarScan 2 [29], Strelka v2.9.10 [30], Platypus

medRxiv preprint doi: https://doi.org/10.1101/2022.07.11.22277322; this version posted July 13, 2022. The copyright holder for this preprint (which was not certified by peer review) is the author/funder, who has granted medRxiv a license to display the preprint in perpetuity. All rights reserved. No reuse allowed without permission.

0.8.1 [31], Mutect2 – part of GATK 4.1.4.1 [28], Somatic Sniper version 1.0.5.0 (SNVs only), and [32] were used for small variant calling and combination of 2 out 5 callers are reported as per Cancer Genome Atlas Research Network recommendations [33]. Variants were filtered using the following criteria:

1. Tcov > 10 & Taf >=0.04 & Ncov > 7 & Naf <= 0.01 & Tac > 4 are set to Pass
2. Common SNPs are eliminated by comparison to snp142.vcf
3. Rare variants found in dbSNP are kept if Naf = 0
4. Variants with Tcov < 20 or Tac < 4 are marked as low_confidence
5. Only variants called by more than 1 caller are reported.
6. Common variables gnomAD v 2.1.1 are excluded.

Variants were annotated using Ensembl Variant Effect Predictor (VEP) [34]. Additional optimization and filtering are applied for INDELS. INDELS in blacklisted regions (https://www.encodeproject.org/annotations/ENCSR636HFF/) and low mappability regions (such as repeat maskers) are excluded as per [35]. Combination of filtered SNV and INDELS are used by maftools R package is used to generate oncoplots and summary plots, as per author's recommendations

https://www.bioconductor.org/packages/release/bioc/vignettes/maftools/inst/doc/maftools.html

All nonsynonymous point mutations identified as above were translated into strings of 17 amino acids with the mutant amino acid situated centrally using a bioinformatics tool called NAseek. A sliding window method is used to identify the 8-11 amino acid substrings within the mutant 17-mer that had a predicted MHC Class I binding affinity of ≤ 2 %Rank to one (or more) of the patient-specific HLA alleles. Binding affinity for the mutant and corresponding wild type

medRxiv preprint doi: https://doi.org/10.1101/2022.07.11.22277322; this version posted July 13, 2022. The copyright holder for this preprint (which was not certified by peer review) is the author/funder, who has granted medRxiv a license to display the preprint in perpetuity. All rights reserved. No reuse allowed without permission.

nonamer is analyzed using NetMHCpan4.0 software. Only neoantigens with a TPM>1 are considered to be expressed.

Allele-specific copy number analysis is done by the FACETS v.6.1 [36]. Allele specific HLA loss is determined using LOHHLA as described before [37].

RNA and TCR ITH scores

Gene- and patient-wise intra-patient heterogeneity scores were calculated using multi-region data. Data was first median-centered to remove any gene-level bias. For each gene, the difference between each pair of samples from the same tumor were calculated. The median difference between the paired-differences was then taken, yielding a gene-specific, patient-specific measure of heterogeneity. This was repeated for all genes, across all tumors, generating a matrix of gene by patient values. Gene intratumor heterogeneity values are summarized as the median value per gene across all tumors in the cohort. Patient intratumor heterogeneity values are summarized as the median value per tumor across all genes. Patient intratumor heterogeneity values represent the expected value of the absolute log2-fold change for a randomly chosen gene within a given tumor.

TCR ITH score is defined as 1 – percentage of shared clonotypes across multiple regions of tumor based on WTS. T cell clones are estimated using MiXCR application on Illumina BaseSpace (http://basespace.illumina.com/apps/). Furthermore, all ITH scores are classified as high versus low using the median as threshold.

Distinction between dedicated TCRseq and TCR clones inferred from RNAseq using MiXCR

medRxiv preprint doi: https://doi.org/10.1101/2022.07.11.22277322; this version posted July 13, 2022. The copyright holder for this preprint (which was not certified by peer review) is the author/funder, who has granted medRxiv a license to display the preprint in perpetuity. All rights reserved. No reuse allowed without permission.

All TCR associated data analysis in this study (including tissue or PBMC) are based on ultra-deep T cell repertoire sequencing (targeted TCRseq) to mitigate undersampling of T cell clones except TCR ITH analysis in Fig. 3b where ITH associated with multiregional sequencing is derived from MiXCR T cell estimates from RNAseq data due to the lack of multiregional TCRseq for all patients.

ccRCC evolutionary subtypes and intra-tumor DNA Heterogeneity Score

DNA ITH score is calculated as the ratio of subclonal to clonal driver genomic alterations including SNVs, INDELs, and SCNA [14]. A genomic alteration is defined to be subclonal if it is present in less than half of the regions collected in each patient. Patients who enough DNA biopsies are collected are classified into 1 of the 7 ccRCC evolutionary subtypes as described before [14]. We used neighbor joining tree construction in ape package in R [38] for reconstruction of tumor clones. TCGA ITH score was obtained from a previous study as measured by the number of clones estimated per sample using PhyloWGS [39]. Briefly, PhyloWGS is a method to infer tumor evolution evolutionary using the relationships between tumor subpopulations based on variant allele frequencies while considering copy number alterations.

HLA and TCR diversity

Shannon entropy is calculated to define TCR diversity [40]. We used MiXCR application on Illumina BaseSpace (http://basespace.illumina.com/apps/) for alignment and T cell clonotype identification. Immunarch (https://immunarch.com/) [41] was used for downstream analysis including visualization and data analysis. Morisita index [42] was used to measure clonotype overlap. HLA diversity index is measured as adopted from [43] as described in [25].

medRxiv preprint doi: https://doi.org/10.1101/2022.07.11.22277322; this version posted July 13, 2022. The copyright holder for this preprint (which was not certified by peer review) is the author/funder, who has granted medRxiv a license to display the preprint in perpetuity. All rights reserved. No reuse allowed without permission.

Neoantigen Depletion

The fraction of neoantigens depleted is defined for each sample where pretreatment data was available. We first calculated the neoantigen depletion as the number of neoantigens that were undetectable after therapy but were detected pretreatment. The fraction of neoantigens depleted was then defined as the ratio of the total number of depleted neoantigens over total pretreatment neoantigens. To distinguish neoantigen depletion due to contraction (immune elimination) from evasion, we exclude any neoantigens that were depleted without the presence of HLA LOH (defects in antigen presentation machinery), or reduced expression i.e., log2(FC)< -1 where FC is the fold change defined as the ratio of post treatment TPM over pretreatment TPM after correction for tumor purity. Conversely, a neoantigen is annotated as deleted due to immune elimination if log2(FC)>=0 and no HLA LOH was detected. Likewise, HERV editing is defined as the median change in the expression of immunogenic HERVs compared to pre-treatment expression. Immunogenic HERVs refers to HERV loci whose expression strongly correlates with TIL abundance, FDR<0.05.

Weighted Gene Co-expression Network Analysis (WGCNA) and gene signature extraction

We performed WGCNA [44] on all samples where the fraction of neoantigens depleted was available similar to previously described [10]. Briefly, genes with low expression values and invariant genes, that is, genes that were expressed in <5% of samples or had s.d. ≤ 1 for expression (log2 TPM) were filtered together with non-coding genes. The soft power of 6 was chosen based on goodness of fit to a scale-free network. We first annotate modules as JAVELIN or angiogenesis according to the Spearman correlation between the module eigengene and JAVELIN or angiogenesis ssGSEA scores (highest correlation is classified as JAVELIN or angiogenesis module). Likewise, among all modules, the module with the highest Spearman correlation with the fraction of neoantigens depleted was annotated as immune escape module

medRxiv preprint doi: https://doi.org/10.1101/2022.07.11.22277322; this version posted July 13, 2022. The copyright holder for this preprint (which was not certified by peer review) is the author/funder, who has granted medRxiv a license to display the preprint in perpetuity. All rights reserved. No reuse allowed without permission.

(85 genes). This 85 genes gene signature was strongly associated with PFS of Avelumab plus Axitinib in JAVELIN Renal 101 (HR=1.45, P=0.02, Extended Data Fig. 11a). To further refine this gene signature, we first sorted genes based on their pairwise spearman correlation (Extended Data Fig. 11b) and then selected genes with the highest spearman correlation such that no genes have a spearman correlation <0.6 (Extended Data Fig. 11c). This reduced the number of genes to total of 12 highly correlated genes known as immune escape signature (TIMP1, PXDN, COL15A1, OLFML2B, COL5A2, DLX5, SOX11, KLHDC8A, UNC5A, ADAMTS14, MMP11, FN1). Several genes (ADAMTS14, MMP11, FN1, COL5A1, COL5A2 and TIMP1) in this signature has previously been described as TGF-β-associated extracellular matrix genes that are linked to immune evasion and immunotherapy failure [45].

Statistical Analysis

All statistical tests were performed in R. To calculate correlations, cor.test with Spearman's method was used. Tests comparing distributions were performed using wilcox.test. All statistical analyses were two-sided and p-values were Benjamini-Hochberg corrected.

Results

The landscape of microenvironmental ITH in ccRCC

To study ITH in ccRCC, we completed ultra-deep (median coverage of 360X) multi-regional whole-exome sequencing and whole-transcriptome sequencing across 142 tumor regions from 29 patients, including 6 untreated and 23 post ICI (see Methods and Table S2). Tumor biopsies were extracted from different regions of the same primary tumor unless specified (Fig. 1a, and b, Table S2). While intra-tumoral genetic heterogeneity in ccRCC is well-

medRxiv preprint doi: https://doi.org/10.1101/2022.07.11.22277322; this version posted July 13, 2022. The copyright holder for this preprint (which was not certified by peer review) is the author/funder, who has granted medRxiv a license to display the preprint in perpetuity. All rights reserved. No reuse allowed without permission.

described[46], comparatively little is known about the extent of microenvironmental heterogeneity and its relationship to other molecular features of the tumor. To measure the extent of intra-tumoral microenvironmental heterogeneity, we leveraged multi-regional WTS of up to 5 regions from 29 patients. Using single sample gene set enrichment analysis (ssGSEA) of established gene signatures, we quantified the expression of several TME gene expression signatures recently proposed as biomarkers of response to ICIs and anti-angiogenic agents [47] (myeloid signature [8], JAVELIN signature [10], and angiogenesis signature, see Methods and Supplementary S3). We confirmed that these RNA signatures accurately quantified the abundance of key immune populations using matched immunofluorescence data, including statistically significant associations between CD31/angiogenesis (p=0.0003), CD8/JAVELIN T cell signature (p = 0.02), and CD68/Myeloid infiltration (p=0.0013) (Fig. S1).

Microenvironmental signatures demonstrated extensive heterogeneity across tumor regions from the same patient (Fig. 2a). While a small number of patients showed relatively uniform immune infiltration (*e.g.,* NIVO02, Fig. 2a), the significantly more common phenomenon was for patients to exhibit regions both above and below the median score for a microenvironmental feature of interest (*e.g.,* angiogenesis in MR03, JAVELIN/Teffector signatures in NIVO22). Using the myeloid signature (which has previously been associated with poor response to ICI) as an example, we observed most patients cannot be uniquely classified to myeloid enriched or depleted across all tumor regions (Fig. 2c). Given that several of these signatures are under active investigation as biomarkers of response to ICI, we investigated more generally how classification of regions into high/low was affected by ITH. Remarkably, in more than half of the patients, clinically relevant signatures (Angiogenesis, T-effector, Myeloid, and JAVELIN) could not be consistently classified as high or low (Fig. 2b, 2 patients (MR05 and NIVO10) were excluded since WTS data of only one region was available).

medRxiv preprint doi: https://doi.org/10.1101/2022.07.11.22277322; this version posted July 13, 2022. The copyright holder for this preprint (which was not certified by peer review) is the author/funder, who has granted medRxiv a license to display the preprint in perpetuity. All rights reserved. No reuse allowed without permission.

We hypothesized elevated microenvironmental heterogeneity may reflect the presence of underlying genomic driver alterations. To test this, we leveraged multi-regional WES data collected for these patients. Frequencies of established ccRCC driver alterations were in agreement with a previous multi-regional study by TRACERx Renal [14] (Fig. 3a). We performed unsupervised hierarchical clustering of major ccRCC driver mutations (i.e., *VHL*, *PBRM1*, *SETD2, BAP1*) and genomic alterations enriched with metastatic disease and ICI response (HLA LOH and CDKN2A/B copy number loss)[37, 43, 48], ultimately identifying two clusters (Fig. 3b, Table S4). We compared the results of these clusters to aggregate, univariate measures of intra-tumoral DNA, RNA, and T-cell receptor (TCR) heterogeneity. Interestingly, one cluster was characterized both by an enrichment of specific genomic alterations (SETD2 mutations, Fisher exact test P=0.002; CDKN2A/B copy number loss, Fisher exact test P=0.0001; HLA LOH, Fisher exact test P=0.0007). This same cluster of patients, which we refer to herein as “ITH-high”, had comparable levels of tumor purity to the other “ITH-low” cluster, but demonstrated elevated ITH at the level of somatic DNA alterations, RNA, and TCR (combined Fisher exact test P=0.0495). Moreover, by classifying patients into previously described ccRCC evolutionary subtypes (Fig. S2), we observed that PBRM1-driven tumors were enriched in the ITH-high cluster (on sample level, Fisher exact test P=0.0018), in agreement with TRACERx Renal [14]. However, this finding must be treated with caution due to our relatively small cohort size as well as low number of regions collected in some patients. These findings were robust to the number of regions collected per tumor, and we found no significant association between ITH and exposure to ICI (Fisher exact test P=0.65, Fig. 3b). Together, our results demonstrate (1) that ITH is not restricted to genomic events, but rather is pervasive in the transcriptome, microenvironment, and immune compartment of ccRCC tumors, and (2) correlates with specific somatic events at the level of individual patients (i.e., PBRM1 and SETD2 mutations, HLA LOH and CDKN2A/B loss).

medRxiv preprint doi: https://doi.org/10.1101/2022.07.11.22277322; this version posted July 13, 2022. The copyright holder for this preprint (which was not certified by peer review) is the author/funder, who has granted medRxiv a license to display the preprint in perpetuity. All rights reserved. No reuse allowed without permission.

ITH-high ccRCC tumors are immunologically distinct

Comparing the TME characteristics of ITH-high and ITH-low patients, we observed that ITH-high tumors (defined as all regions belonging to a patient who is classified as ITH-high) were characterized by high myeloid and low T cell effector (Teff) signatures (Fig. 3c). Similarly, a signature associated with antigen presentation (APM)[3] was downregulated in ITH-high patients, consistent with elevated levels of HLA LOH in the ITH-high subtype. To validate if genomic features uniquely characterizing ITH-high tumors (HLA LOH and CDKN2A/B loss) might be more generally associated with myeloid infiltration in a large, independent cohort, we obtained DNA and RNA sequencing data from the TCGA KIRC study and scored samples by the presence of CDKN2A/B loss, ITH (as measured by the number of clones estimated per sample using PhyloWGS, see Methods), and myeloid infiltration. This analysis confirmed that in ccRCC, CDKN2A/B loss was associated with higher levels of ITH ($P=3x10^{-5}$) and higher myeloid infiltration ($P=7x10^{-5}$) (Fig. 3d). However, the association between genomic ITH and myeloid infiltration did not reach statistical significance in TCGA KIRC cohort suggesting the association between myeloid infiltration and ITH is likely indirect through certain genomic events such as CDKN2A/B loss.

The findings above suggested that ITH-high tumors may be distinct in their immunophenotype, including in the diversity of their T cell repertoire. We therefore investigated the association between ITH and T cell diversity both peripherally and within the tumor. To do so, we compared the overlap between tissue-resident and peripheral T cells. Repertoire overlap analysis (Fig. S3) illustrated a high degree of shared clonotypes across different tumor regions from the same patient, but a lack of shared clonotypes across patients. ITH-high patients demonstrated a significantly lower peripheral TCR diversity, richness and clone count compared to ITH-low patients (Fig. 3e), suggesting that elevated heterogeneity in the primary tumor is associated with reduced peripheral immunologic diversity in a manner that is consistent with

medRxiv preprint doi: https://doi.org/10.1101/2022.07.11.22277322; this version posted July 13, 2022. The copyright holder for this preprint (which was not certified by peer review) is the author/funder, who has granted medRxiv a license to display the preprint in perpetuity. All rights reserved. No reuse allowed without permission.

reports in other diseases [49]. To allow a fair comparison of samples with different number of T cells and account for TCR subsampling, we also studied rarefaction curves and estimated TCR diversity by sequentially resampling TCR clonotypes and computing mean number of unique clones [50]. Estimated diversity using rarefaction curves led to a similar conclusion confirming the observed differences in the TCR diversity are unlikely to be due to artifacts in T cell subsampling (Fig. S3b). Together, the above data argue that elevated molecular heterogeneity in ccRCC tumors is associated with a distinct microenvironmental and immunologic phenotype.

ICI therapy is associated with loss of putative neoantigens and HLA LOH

The clinical management of ccRCC (for which pre-surgical biopsies are often not indicated or used) makes serial profiling of primary tumors on therapy challenging, rendering our understanding of how ICI may remodel tumor physiology incomplete. To overcome this challenge, we took advantage of 16 patients from our neoadjuvant nivolumab clinical trial who had WES performed on their pre-treatment biopsies. This offered a unique opportunity to interrogate both genomic adaptations (including both somatic mutations as well as the expression of potentially immunogenic endogenous retroviral elements, HERVs) to ICI therapy, as well as immunologic changes in the T cell repertoire.

Focusing first on genetic alterations, we anticipated that ICI administration would lead to elimination of some tumor clones and therefore a contraction in total mutation count. However, we observed no consistent trend in the change of either SNV or indel mutational count following ICI therapy (Fig. S4). Nevertheless, the number of non-synonymous SNVs that were predicted to bind to MHC complex *in silico* was consistently reduced across all patients and all biopsies except for NIVO03 (Fig. S4 and Fig. 4a). An opposite trend was observed in the number of putative non-binders, suggesting a selection in favor of non-neoantigenic mutations by tumor during clonal evolution (Fig. 4a).

medRxiv preprint doi: https://doi.org/10.1101/2022.07.11.22277322; this version posted July 13, 2022. The copyright holder for this preprint (which was not certified by peer review) is the author/funder, who has granted medRxiv a license to display the preprint in perpetuity. All rights reserved. No reuse allowed without permission.

In order to characterize the clonality of putative neoantigen depletion across distinct tumor regions, we counted all 8-11 amino-acid-long putative neoantigens seen prior to treatment but deleted in at least one biopsy after treatment. Among 7 patients with at least 4 tumor regions sequenced, we observed an enrichment for putative neoantigen depletion across 4 or more sites (Fig. 4b). Focusing on patient NIVO20, all 6 identified depleted putative neoantigens were deleted in at least 4 regions, suggesting putative neoantigen depletion is a clonal event (Fig. 4c). Genes expressing these depleted neoantigens demonstrated a 2-3-fold reduction in expression related to pre-treatment biopsy (NIVO20-RA/RB/RC/RD/RE vs NIVO20-BX) (Fig. 4d). Together with the data above, these observations suggest that ICI therapy in ccRCC is associated with the clonal loss of mutations with elevated immunogenicity.

Premised on prior reports [51] of the increased immunogenicity of hydrophobic residues, we sought to determine whether a selective pressure exists on certain neoantigens. We compared the number of amino acids preserved versus depleted upon immunotherapy, and noticed a strong selection against Phenylalanine (F, extremely hydrophobic) in favor of Arginine (R, extremely hydrophilic) and Glutamic acid (E, extremely hydrophilic) in our cohort (Fig. 4e).

We next examined the magnitude of putative neoantigen depletion in each patient by measuring the average number of putative neoantigens deleted per biopsy (i.e., the ratio of the deleted neoantigens in a treated region compared to pre-treatment over the total number of pre-treatment neoantigens). We observed that the fraction of neoantigens depleted was strongly associated with myeloid-high regions (n = 16 patients whose pre-ICI treatment WES data was available, Fig. 4f). The association between myeloid activation and neoantigen depletion remained strong when total number of neoantigens depleted was used (instead of fraction) (Fig. S5b) or when putative neoantigen (transcriptional) expression was taken into account (n = 7 patients whose pre-treatment WTS data was available, Fig. 4g) and was not affected by variation in tumor purity (Fig. S5). Furthermore, the correlation between the degree of neoantigen depletion

medRxiv preprint doi: https://doi.org/10.1101/2022.07.11.22277322; this version posted July 13, 2022. The copyright holder for this preprint (which was not certified by peer review) is the author/funder, who has granted medRxiv a license to display the preprint in perpetuity. All rights reserved. No reuse allowed without permission.

and myeloid infiltration was also evident when examining different regions of individual patients, where highly depleted regions were associated with the highest myeloid and lowest ImmuneScore (Fig. 4g).

A recent study [52] identified tumor infiltrating lymphocyte specific HERV epitopes that are translated, can bind to MHC I complex, and induce high-avidity cytotoxic T cells. In [52] as well as other previous reports [53], over expression of HERVs on tumor cells has been reported and a link to ICI response has been documented [54]. To interrogate other tumor intrinsic features associated with immune response in our cohort we utilized our deep RNA sequencing (~200 millions read/library) to quantify HERV expression. HERVs were overexpressed in tumors compared to normal tissues in our cohort (Fig. 4h), and median HERV (median of all HERV loci investigated) was correlated to angiogenic expression (Fig. S7a). Notably, PBRM1 mutations, which lead to further HIF upregulation [55] and angiogenic expression [56, 57], were also positively associated with HERV (Fig. S7b), consistent with a recent report [58]. In agreement with [54] we then confirmed the association between the median expression of different HERV loci and TIL abundance (Fig. S7a). Median HERV was anti-correlated with tumor purity; however, the association between HERV expression and TIL abundance remained valid even when HERV expression was corrected for tumor purity (Fig. S7a). Conversely, we observed a significant reduction in HERV expression an observation akin to reduction in neoantigens (Fig. 4i). Likewise, we observed a strong correlation between HERV editing (i.e., change in the expression of immunogenic HERV loci after treatment, see Methods) and myeloid signature further highlighting the association between neoantigen depletion and myeloid enrichment (Fig. 4j). Due to the limitations of HERV quantification using WTS, we could not rule out that a strong correlation between HERV and TIL abundance might be due to expression of HERV on immune cells. However, the expression of HERV on ccRCC tumor cells has been previously shown [59] and their immunogenicity is well-established [52]. Nevertheless, rigorous determination in future

medRxiv preprint doi: https://doi.org/10.1101/2022.07.11.22277322; this version posted July 13, 2022. The copyright holder for this preprint (which was not certified by peer review) is the author/funder, who has granted medRxiv a license to display the preprint in perpetuity. All rights reserved. No reuse allowed without permission.

studies of cell-specific expression of HERVs will be critical to understanding their putative association with ICI response.

Finally, using TCRseq of tissue resident and peripheral T cells, we investigated the impact of ICI and neoantigen depletion on T cell diversity. Focusing again on patient NIVO20 where TCR data of multiple regions of pre-treatment and ICI treated tumor were available, we evaluated the degree of overlap between T cell clonotypes at different regions and time points i.e., pre-treatment, on-therapy, and post ICI treatment (Fig. 4k). Tracking dominant tissue resident T cell clonotypes, we noticed a substantial depletion of dominant T cell clones upon ICI therapy (Fig. 4k). This observation was mirrored across our entire cohort, where we observed a strong negative association between peripheral TCR diversity and neoantigen depletion and allele specific HLA loss across the entire cohort where PBMC TCRseq data was collected (Fig. 4l, m). Together, if validated using future mechanistic experiments, our findings suggest that neoantigen depletion in primary ccRCC tumors is associated with peripheral loss of neoantigen reactive T cells. However, at this point, no causal relationship between neoantigen loss and TCR diversity can be drawn.

Subclonal evolution underlies immune escape

In order to understand the immunologic mechanisms driving subclonal evolution after ICI, we investigated in detail patients whose tumors underwent subclonal immunoediting in distinct regions. Strikingly, subclonal reconstruction revealed recurrent subclonal evolution of HLA LOH and CDKN2A/B loss following ICI therapy (Fig. 5a). Notably, we observed HLA LOH and CDKN2A/B loss co-occur in 9 patients (Fisher exact test P=0.003) and most tumor regions (Fisher exact $P=5\times10^{-7}$) (Fig. 5b). Strikingly, comparing the untreated and treated regions, we only observed a significant immunological response (as measured by Th1 response) in regions without CDKN2A/B loss or HLA LOH (Fig. 5c), suggesting that HLALOH or CDKN2A/B loss are subclonal determinants of response to ICI [37, 43, 48]. This is consistent with recently published data [49]

medRxiv preprint doi: https://doi.org/10.1101/2022.07.11.22277322; this version posted July 13, 2022. The copyright holder for this preprint (which was not certified by peer review) is the author/funder, who has granted medRxiv a license to display the preprint in perpetuity. All rights reserved. No reuse allowed without permission.

504 indicating the loss of 9p21 - encompassing CDKN2A/B – confers a cold tumor immune
505 microenvironment and resistance to ICI. In that study, Han *et al.* [49] linked 9p21 loss to a
506 decreased abundance of B, T, CD8 T, NK cells and cytotoxic lymphocytes, and an increased
507 fractions of macrophages, as well as reduced TCR CDR3 repertoire abundance and diversity. We
508 interpret our observations to mean that immuno-editing occurs under selective pressure by which
509 certain tumor subclones transform to a less immunogenic phenotype through HLA LOH and
510 CDKN2A/B loss, and that this subclonal selection can produce a highly heterogenous TME.

511 To further shed light on the how tumor evolution can transform TME, we sought to analyze
512 the spatial distribution of TILs within the TME and their interaction with the stromal compartment
513 using immunohistochemical data. Following A.W. Zhang and colleagues [60], a dedicated
514 genitourinary pathologist classified tumor regions into 3 subtypes according to the co-localization
515 of tumor infiltrating lymphocytes and tumor cells: N-TIL (tumors sparsely infiltrated by TILs), S-
516 TIL (tumors dominated by stromal TILs), and ES-TIL (tumors with substantial levels of both
517 epithelial and stromal TILs) (Fig. 5d). We observed that an ES-TIL enriched TME is strongly
518 associated with regions with HLA LOH (ES=4, N=7, S=5 compared to ES=2, N=32, S=21 in HLA
519 intact regions, Fisher`s exact test P = 0.036) or loss of CDKN2A/B (ES=4, N=7, S=9 compared to
520 ES=2, N=32, S=17 in regions without loss of CDKN2A/B, Fisher`s exact test P = 0.03) whereas
521 N-TIL pathology is linked with regions with no HLA LOH and no CDKN2A/B loss across the cohort.
522 These findings suggest that despite abundant TILs, post-ICI ES-TIL are associated with tumor
523 clones that have evolved genetic mechanisms for evasion of the immune response (HLA LOH
524 and/or CDKN2A/B loss). However, future mechanistic studies are needed to pinpoint the primary
525 genomic event that transforms the ccRCC TME into a cold niche.

526

527 **An adverse ccRCC TME is enriched stroma and myeloid signatures**

medRxiv preprint doi: https://doi.org/10.1101/2022.07.11.22277322; this version posted July 13, 2022. The copyright holder for this preprint (which was not certified by peer review) is the author/funder, who has granted medRxiv a license to display the preprint in perpetuity. All rights reserved. No reuse allowed without permission.

We hypothesized that neoantigen depletion could be associated with a specific transcriptional signature, akin to those identified in clinical trial settings as biomarkers for response to ICI in ccRCC. To identify such a signature, we performed unsupervised Weighted Gene Co-expression Network Analysis (WGCNA) [44] to reconstruct modules from our transcriptomic samples similar to [10] (Fig. 6a). Reassuringly, we identified two gene expression modules #7 and #4 reflecting established microenvironmental features associated with therapeutic response in ccRCC: immune inflammatory response ("JAVELIN-like" signature) and "angiogenesis-like" (Fig. 6a, b). We next assessed the correlation between the expression of each WGCNA gene module and neoantigen depletion. While the JAVELIN-like and angiogenesis-like modules showed no association with neoantigen depletion, module 16 demonstrated the strongest association (Fig. 6a). Correlation analysis with previously known gene expression signatures illustrated that module 16 (which we refer to as an "*Immune Escape*" signature) was strongly associated with myeloid and stroma features of TME. The Immune Escape signature also resembled a recently described pan-cancer TGFβ signature derived in a previous study [45] which was linked to cancer-associated fibroblasts enriched in immune evasion and immunotherapy failure. However, no association between the Immune Escape signature and treatment status was observed (Wilcox P=0.79) (Fig. S8).

To reveal the primary cellular populations driving the Immune Escape signature in the ccRCC TME, we leveraged scRNAseq from multiple tumor regions, lymph node, normal kidney, and peripheral blood of two ICI-naïve and four ICI-treated patients [15] (n=167283 single cells) (Fig. 1c). We identified 28 clusters (Fig. 6c) using Louvain clustering [61, 62] and each cluster was annotated based on our previous study [15]. As expected, scRNAseq revealed enrichment of this signature in renal epithelium, tumor stroma as well as tumor associated macrophages (TAMs) and monocytes (Fig. 6c). Hence, both scRNAseq and histopathological evaluation further confirmed the association between Immune Escape and neoantigen depletion (Fig. 6a, Spearman

medRxiv preprint doi: https://doi.org/10.1101/2022.07.11.22277322; this version posted July 13, 2022. The copyright holder for this preprint (which was not certified by peer review) is the author/funder, who has granted medRxiv a license to display the preprint in perpetuity. All rights reserved. No reuse allowed without permission.

553 correlation = 0.6), ITH (Fig. 6d, Wilcox P=0.003), myeloid activation (Fig. 6b, Spearman
554 correlation = 0.8) and with stroma, and renal epithelium histopathology (Fig. 5d and Fig. 6e, f).

555

556 **Immune Escape correlates with clinical outcome to ICI therapy**

557 Several previous studies have associated signatures of Immune Escape with poor clinical
558 outcome in ICI treated patients [63]. Thus, we evaluated whether our Immune Escape signature
559 can correlate with clinical outcome to ICI treatment. We obtained publicly available RNAseq data
560 for several clinical trials including phase 3 JAVELIN Renal 101 trial [10] – a phase III randomized
561 anti-PD-L1 (avelumab) plus tyrosine kinase inhibitor (TKI, axitinib) versus multi-target TKI
562 (sunitinib), IMmotion151 [64] – a phase III trial comparing anti-PDL1 (atezolizumab) plus anti-
563 angeniogenesis agent (bevacizumab) versus TKI (sunitinib) in first-line metastatic renal cell
564 carcinoma, CheckMate 009/010 – a phase I/II, aPD-1 (nivolumab) treated, and CheckMate 025 –
565 a phase III randomized mTOR inhibitor (everolimus) versus aPD-1 [9]. We stratified patients by
566 the median score (see Methods) of the 3 gene signatures obtained in our study (i.e., module
567 4/JAVELIN_like, 7/angiogenesis-like, and 16/immune escape.

568 The Immune Escape signature was strongly associated with the response to all three ICI
569 regimens (avelumab plus axitinib HR=1.53 P=0.008, atezolizumab plus bevacizumab HR=1.35
570 P=0.019 and nivolumab HR=1.45 P=0.02, Fig. 7 and Fig. S9). In contrast, the JAVELIN-like
571 inflammatory signature was strongly associated with clinical outcome to avelumab plus axitinib
572 (HR=0.64 P=0.006), but no association with clinical benefit was found between atezolizumab plus
573 bevacizumab (HR=0.82 P=0.126) or nivolumab treatment (HR=0.97 P=0.823) (Fig. 7). Similarly,
574 the angiogenesis-like signature was strongly correlated with the response to sunitinib in both
575 IMmotion151 (HR=0.48 P<0.001) and JAVELIN Renal 101 (HR=0.68 P=0.008) as expected, but
576 not with ICI-associated regimens. Associations between the Immune Escape signature and
577 therapeutic response remained valid even when thresholds other than median were used to

medRxiv preprint doi: https://doi.org/10.1101/2022.07.11.22277322; this version posted July 13, 2022. The copyright holder for this preprint (which was not certified by peer review) is the author/funder, who has granted medRxiv a license to display the preprint in perpetuity. All rights reserved. No reuse allowed without permission.

define immune escape high and low (Fig. S10). Even though the Immune Escape signature was also associated with response to sunitinib in JAVELIN Renal 101, no association between sunitinib response or mTOR inhibition was observed in IMmotion151 and CheckMate 025. Overall, this analysis suggests that a transcriptional signature associated the tendency to lose putative neoantigens after ICI is associated with response to combination ICI therapy and nominates a new potential biomarker for this therapeutic regimen.

Discussion

Here we used spatiotemporal, multimodal profiling to investigate the link tumor genomics, microenvironmental heterogeneity, peripheral immune response, and eventual immune escape in advanced and metastatic ccRCC. The fundamental discovery of our analysis is that ITH manifests well beyond the tumor genome and produces highly heterogeneous immune microenvironments in the tumor. Our findings clearly suggest that the ccRCC genome and microenvironment co-evolve, and that loss of putative neo-antigens (including SNVs, indels, and HERVs) is associated with a qualitatively myeloid-high environment and the loss of HLA and CDKN2A/B. These distinct genomic alterations are also associated with more peripheral changes, i.e., reduced T cell clonal diversity in the peripheral circulation.

Emerging data on biomarkers of response to ICI in ccRCC has identified two potentially paradoxical observations: first, that TIL abundance alone is an insufficient predictor of ICI response [9], and second, that the presence of myeloid cells correlate with resistance to both ICI and anti-VEGF treatments. Strikingly, we observed that high myeloid score tumors were associated with neoantigen depletion which could, in principle, render ICI treatment ineffective. In agreement with this, we derived a transcriptomic signature associated with neoantigen depletion and Immune Escape, which was expressed in renal epithelium, tumor stroma as well as tumor associated macrophages (TAMs) and monocytes. This Immune Escape signature was associated

medRxiv preprint doi: https://doi.org/10.1101/2022.07.11.22277322; this version posted July 13, 2022. The copyright holder for this preprint (which was not certified by peer review) is the author/funder, who has granted medRxiv a license to display the preprint in perpetuity. All rights reserved. No reuse allowed without permission.

603 with response to several ICI regiments in published clinical trials. In total, these findings suggest
604 that myeloid cells are associated with tumor clones that have evolved mechanisms to escape
605 anti-tumor immune responses. Critically, such a hypothetic model requires detailed work and
606 mechanistic validation in immunocompetent systems, which we are actively developing.

607 Why do regions with neoantigen depletion demonstrate elevation of myeloid cells but not
608 cytotoxic T cells that would presumably eliminate tumor clones? Cancer immunoediting proceeds
609 through three phases: elimination, equilibrium and escape [65]. Throughout these phases, tumor
610 immunogenicity evolves, and thereby, despite possible initial response to therapy, acquires
611 immunosuppressive mechanisms that may enable disease progression. Our data suggests that
612 myeloid-high, neoantigen-depleted tumor regions historically experienced a cytotoxic T cell
613 response, which prompted the selection of tumor clones losing neoantigens and/or
614 HLA/CDKN2A/B. Such a loss of target antigens through HLA LOH or neoantigen depletion would
615 result in loss of antigen-TCR stimulation, leading to death of the corresponding neoantigen
616 reactive T cells (Fig. 8). Importantly, as with other findings in this analysis, the association
617 between neoantigen loss and myeloid activation observed in our data remains purely correlative,
618 and future studies will be necessary to mechanistically establish how immune evasion
619 spatiotemporally evolves in ccRCC following ICI therapy.

620 Our multi-regional data also has significant implications for biomarker development. We
621 demonstrated that TME markers of response such as JAVELIN and myeloid scores can be
622 heterogenous within tumors regions (Fig. 2). This underscores the importance of accounting for
623 ITH when these signatures are used for patient selection for a specific therapy and longitudinal
624 monitoring of therapies. Given recent data that ICI may have a role in adjuvant therapy following
625 nephrectomy for high-risk disease, our data would suggest that several regions of the primary
626 tumor should be sampled specially in the presence of ITH associated genomic alterations (e.g.,
627 HLA LOH and CDKN2A/B loss). An intriguing finding was a trend towards lower ITH in ICI treated

medRxiv preprint doi: https://doi.org/10.1101/2022.07.11.22277322; this version posted July 13, 2022. The copyright holder for this preprint (which was not certified by peer review) is the author/funder, who has granted medRxiv a license to display the preprint in perpetuity. All rights reserved. No reuse allowed without permission.

tumors, even though this observation did not reach statistical significance. If validated in other studies, this in part can be attributed to outgrowth of few non-immunogenic tumor subclones that managed to escape immune surveillance upon ICI treatment.

An important limitation of this study is that TME heterogeneity of metastatic disease was not assessed and may be less of an issue in biomarker development. Our study has several other potential limitations including its small sample size. To overcome this shortcoming, we validated several of our major findings in several independent cohorts. Another potential limitation of our study is the unavailability pre-treatment multi-regional sequencing data. However, inclusion of multi-regional data from 6 untreated patients allowed us to account for ITH in untreated tumors. Moreover, our neoadjuvant cohort was treated with single agent nivolumab over a short course which may not reflect the TME, and genomic changes induced by more potent combination strategies. Finally, we portrayed the characteristics of an adverse TME which may contribute to ICI resistance. Our study clearly demonstrates the interplay between genomic events and TME transformation from a cytotoxic to a cold immuno-phenotype. However, these findings remain purely an association of several contributing factors to ICI resistant and the exact causative hierarchy of events requires further investigation.

In conclusion, we find distinct genomic event enriched in immune escape tumor microenvironment in ccRCC both across and within tumors. Our findings have implications for future biomarker development for ICI response across ccRCC and other solid tumors.

Availability of data and materials

No new code was generated. All data generated in this study are provided in Extended Data Table and Figures or available upon reasonable request from corresponding author.

medRxiv preprint doi: https://doi.org/10.1101/2022.07.11.22277322; this version posted July 13, 2022. The copyright holder for this preprint (which was not certified by peer review) is the author/funder, who has granted medRxiv a license to display the preprint in perpetuity. All rights reserved. No reuse allowed without permission.

Abbreviations

TCGA: The Cancer Genome Atlas

WES: Whole-exome sequencing

WTS: Whole-transcriptome sequencing

SCNA: Somatic copy number alterations

LOH: Loss of heterozygosity

ITH: Intra-tumoral heterogeneity

TCR: T cell receptor

ccRCC: clear cell Renal Cell Carcinoma

TME: Tumor microenvironment

ICI: Immune checkpoint inhibitor

TKI: Tyrosine kinase inhibitor

HERV: Human endogenous retrovirus

PBMC: peripheral blood mononuclear cells

TIL: Tumor infiltrating lymphocytes

WGCNA: Weighted gene co-expression network analysis

ssGSEA: single sample gene set enrichment analysis

References

1. Liu X-D, Hoang A, Zhou L, Kalra S, Yetil A, Sun M, Ding Z, Zhang X, Bai S, German P: **Resistance to antiangiogenic therapy is associated with an immunosuppressive**

medRxiv preprint doi: https://doi.org/10.1101/2022.07.11.22277322; this version posted July 13, 2022. The copyright holder for this preprint (which was not certified by peer review) is the author/funder, who has granted medRxiv a license to display the preprint in perpetuity. All rights reserved. No reuse allowed without permission.

tumor microenvironment in metastatic renal cell carcinoma. *Cancer immunology research* 2015, **3:**1017-1029.

2. Rooney MS, Shukla SA, Wu CJ, Getz G, Hacohen N: **Molecular and genetic properties of tumors associated with local immune cytolytic activity.** *Cell* 2015, **160:**48-61.
3. Şenbabaoğlu Y, Gejman RS, Winer AG, Liu M, Van Allen EM, de Velasco G, Miao D, Ostrovnaya I, Drill E, Luna A: **Tumor immune microenvironment characterization in clear cell renal cell carcinoma identifies prognostic and immunotherapeutically relevant messenger RNA signatures.** *Genome biology* 2016, **17:**1-25.
4. Snyder A, Makarov V, Merghoub T, Yuan J, Zaretsky JM, Desrichard A, Walsh LA, Postow MA, Wong P, Ho TS: **Genetic basis for clinical response to CTLA-4 blockade in melanoma.** *New England Journal of Medicine* 2014, **371:**2189-2199.
5. Le DT, Durham JN, Smith KN, Wang H, Bartlett BR, Aulakh LK, Lu S, Kemberling H, Wilt C, Luber BS: **Mismatch repair deficiency predicts response of solid tumors to PD-1 blockade.** *Science* 2017, **357:**409-413.
6. Samstein RM, Lee C-H, Shoushtari AN, Hellmann MD, Shen R, Janjigian YY, Barron DA, Zehir A, Jordan EJ, Omuro A: **Tumor mutational load predicts survival after immunotherapy across multiple cancer types.** *Nature genetics* 2019, **51:**202-206.
7. Havel JJ, Chowell D, Chan TA: **The evolving landscape of biomarkers for checkpoint inhibitor immunotherapy.** *Nature Reviews Cancer* 2019, **19:**133-150.
8. McDermott DF, Huseni MA, Atkins MB, Motzer RJ, Rini BI, Escudier B, Fong L, Joseph RW, Pal SK, Reeves JA: **Clinical activity and molecular correlates of response to atezolizumab alone or in combination with bevacizumab versus sunitinib in renal cell carcinoma.** *Nature medicine* 2018, **24:**749-757.
9. Braun DA, Hou Y, Bakouny Z, Ficial M, Sant'Angelo M, Forman J, Ross-Macdonald P, Berger AC, Jegede OA, Elagina L: **Interplay of somatic alterations and immune infiltration modulates response to PD-1 blockade in advanced clear cell renal cell carcinoma.** *Nature medicine* 2020, **26:**909-918.
10. Motzer RJ, Robbins PB, Powles T, Albiges L, Haanen JB, Larkin J, Mu XJ, Ching KA, Uemura M, Pal SK: **Avelumab plus axitinib versus sunitinib in advanced renal cell carcinoma: Biomarker analysis of the phase 3 JAVELIN Renal 101 trial.** *Nature medicine* 2020, **26:**1733-1741.
11. Motzer RJ, Escudier B, McDermott DF, George S, Hammers HJ, Srinivas S, Tykodi SS, Sosman JA, Procopio G, Plimack ER: **Nivolumab versus everolimus in advanced renal-cell carcinoma.** *New England Journal of Medicine* 2015, **373:**1803-1813.
12. Yarchoan M, Hopkins A, Jaffee EM: **Tumor mutational burden and response rate to PD-1 inhibition.** *The New England journal of medicine* 2017, **377:**2500.
13. Rini BI, Plimack ER, Stus V, Gafanov R, Hawkins R, Nosov D, Pouliot F, Alekseev B, Soulières D, Melichar B: **Pembrolizumab plus axitinib versus sunitinib for advanced renal-cell carcinoma.** *New England Journal of Medicine* 2019, **380:**1116-1127.
14. Turajlic S, Xu H, Litchfield K, Rowan A, Horswell S, Chambers T, O'Brien T, Lopez JI, Watkins TB, Nicol D: **Deterministic evolutionary trajectories influence primary tumor growth: TRACERx renal.** *Cell* 2018, **173:**595-610. e511.
15. Krishna C, DiNatale RG, Kuo F, Srivastava RM, Vuong L, Chowell D, Gupta S, Vanderbilt C, Purohit TA, Liu M: **Single-cell sequencing links multiregional immune landscapes and tissue-resident T cells in ccRCC to tumor topology and therapy efficacy.** *Cancer Cell* 2021.
16. Au L, Hatipoglu E, de Massy MR, Litchfield K, Beattie G, Rowan A, Schnidrig D, Thompson R, Byrne F, Horswell S: **Determinants of anti-PD-1 response and resistance in clear cell renal cell carcinoma.** *Cancer cell* 2021, **39:**1497-1518. e1411.

medRxiv preprint doi: https://doi.org/10.1101/2022.07.11.22277322; this version posted July 13, 2022. The copyright holder for this preprint (which was not certified by peer review) is the author/funder, who has granted medRxiv a license to display the preprint in perpetuity. All rights reserved. No reuse allowed without permission.

17. Dobin A, Davis CA, Schlesinger F, Drenkow J, Zaleski C, Jha S, Batut P, Chaisson M, Gingeras TR: **STAR: ultrafast universal RNA-seq aligner.** *Bioinformatics* 2013, **29:**15-21.
18. Lawrence M, Huber W, Pages H, Aboyoun P, Carlson M, Gentleman R, Morgan MT, Carey VJ: **Software for computing and annotating genomic ranges.** *PLoS Comput Biol* 2013, **9:**e1003118.
19. Karolchik D, Baertsch R, Diekhans M, Furey TS, Hinrichs A, Lu Y, Roskin KM, Schwartz M, Sugnet CW, Thomas DJ: **The UCSC genome browser database.** *Nucleic acids research* 2003, **31:**51-54.
20. Love MI, Huber W, Anders S: **Moderated estimation of fold change and dispersion for RNA-seq data with DESeq2.** *Genome biology* 2014, **15:**1-21.
21. Yoshihara K, Shahmoradgoli M, Martínez E, Vegesna R, Kim H, Torres-Garcia W, Treviño V, Shen H, Laird PW, Levine DA: **Inferring tumour purity and stromal and immune cell admixture from expression data.** *Nature communications* 2013, **4:**1-11.
22. Barbie DA, Tamayo P, Boehm JS, Kim SY, Moody SE, Dunn IF, Schinzel AC, Sandy P, Meylan E, Scholl C: **Systematic RNA interference reveals that oncogenic KRAS-driven cancers require TBK1.** *Nature* 2009, **462:**108-112.
23. Newman AM, Liu CL, Green MR, Gentles AJ, Feng W, Xu Y, Hoang CD, Diehn M, Alizadeh AA: **Robust enumeration of cell subsets from tissue expression profiles.** *Nature methods* 2015, **12:**453-457.
24. Bindea G, Mlecnik B, Tosolini M, Kirilovsky A, Waldner M, Obenauf AC, Angell H, Fredriksen T, Lafontaine L, Berger A: **Spatiotemporal dynamics of intratumoral immune cells reveal the immune landscape in human cancer.** *Immunity* 2013, **39:**782-795.
25. Golkaram M, Salmans ML, Kaplan S, Vijayaraghavan R, Martins M, Khan N, Garbutt C, Wise A, Yao J, Casimiro S: **HERVs establish a distinct molecular subtype in stage II/III colorectal cancer with poor outcome.** *NPJ genomic medicine* 2021, **6:**1-11.
26. Li H, Durbin R: **Fast and accurate short read alignment with Burrows–Wheeler transform.** *bioinformatics* 2009, **25:**1754-1760.
27. McKenna A, Hanna M, Banks E, Sivachenko A, Cibulskis K, Kernytsky A, Garimella K, Altshuler D, Gabriel S, Daly M: **The Genome Analysis Toolkit: a MapReduce framework for analyzing next-generation DNA sequencing data.** *Genome research* 2010, **20:**1297-1303.
28. DePristo MA, Banks E, Poplin R, Garimella KV, Maguire JR, Hartl C, Philippakis AA, Del Angel G, Rivas MA, Hanna M: **A framework for variation discovery and genotyping using next-generation DNA sequencing data.** *Nature genetics* 2011, **43:**491.
29. Koboldt DC, Zhang Q, Larson DE, Shen D, McLellan MD, Lin L, Miller CA, Mardis ER, Ding L, Wilson RK: **VarScan 2: somatic mutation and copy number alteration discovery in cancer by exome sequencing.** *Genome research* 2012, **22:**568-576.
30. Kim S, Scheffler K, Halpern AL, Bekritsky MA, Noh E, Källberg M, Chen X, Kim Y, Beyter D, Krusche P: **Strelka2: fast and accurate calling of germline and somatic variants.** *Nature methods* 2018, **15:**591-594.
31. Rimmer A, Phan H, Mathieson I, Iqbal Z, Twigg SR, Wilkie AO, McVean G, Lunter G: **Integrating mapping-, assembly-and haplotype-based approaches for calling variants in clinical sequencing applications.** *Nature genetics* 2014, **46:**912-918.
32. Larson DE, Harris CC, Chen K, Koboldt DC, Abbott TE, Dooling DJ, Ley TJ, Mardis ER, Wilson RK, Ding L: **SomaticSniper: identification of somatic point mutations in whole genome sequencing data.** *Bioinformatics* 2012, **28:**311-317.
33. Ellrott K, Bailey MH, Saksena G, Covington KR, Kandoth C, Stewart C, Hess J, Ma S, Chiotti KE, McLellan M: **Scalable open science approach for mutation calling of**

medRxiv preprint doi: https://doi.org/10.1101/2022.07.11.22277322; this version posted July 13, 2022. The copyright holder for this preprint (which was not certified by peer review) is the author/funder, who has granted medRxiv a license to display the preprint in perpetuity. All rights reserved. No reuse allowed without permission.

tumor exomes using multiple genomic pipelines. *Cell systems* 2018, **6:**271-281. e277.

34. McLaren W, Gil L, Hunt SE, Riat HS, Ritchie GR, Thormann A, Flicek P, Cunningham F: **The ensembl variant effect predictor.** *Genome biology* 2016, **17:**1-14.
35. Amemiya HM, Kundaje A, Boyle AP: **The ENCODE blacklist: identification of problematic regions of the genome.** *Scientific reports* 2019, **9:**1-5.
36. Shen R, Seshan VE: **FACETS: allele-specific copy number and clonal heterogeneity analysis tool for high-throughput DNA sequencing.** *Nucleic acids research* 2016, **44:**e131-e131.
37. McGranahan N, Rosenthal R, Hiley CT, Rowan AJ, Watkins TB, Wilson GA, Birkbak NJ, Veeriah S, Van Loo P, Herrero J: **Allele-specific HLA loss and immune escape in lung cancer evolution.** *Cell* 2017, **171:**1259-1271. e1211.
38. Paradis E, Claude J, Strimmer K: **APE: analyses of phylogenetics and evolution in R language.** *Bioinformatics* 2004, **20:**289-290.
39. Raynaud F, Mina M, Tavernari D, Ciriello G: **Pan-cancer inference of intra-tumor heterogeneity reveals associations with different forms of genomic instability.** *PLoS genetics* 2018, **14:**e1007669.
40. Wu TD, Madireddi S, de Almeida PE, Banchereau R, Chen Y-JJ, Chitre AS, Chiang EY, Iftikhar H, O'Gorman WE, Au-Yeung A: **Peripheral T cell expansion predicts tumour infiltration and clinical response.** *Nature* 2020, **579:**274-278.
41. Nazarov V: **immunarch. bot & Eugene Rumynskiy. immunomind/immunarch: 0.6. 5: Basic single-cell support.** Zenodo; 2020.
42. Horn HS: **Measurement of" overlap" in comparative ecological studies.** *The American Naturalist* 1966, **100:**419-424.
43. Chowell D, Krishna C, Pierini F, Makarov V, Rizvi NA, Kuo F, Morris LG, Riaz N, Lenz TL, Chan TA: **Evolutionary divergence of HLA class I genotype impacts efficacy of cancer immunotherapy.** *Nature medicine* 2019, **25:**1715-1720.
44. Langfelder P, Horvath S: **WGCNA: an R package for weighted correlation network analysis.** *BMC bioinformatics* 2008, **9:**1-13.
45. Chakravarthy A, Khan L, Bensler NP, Bose P, De Carvalho DD: **TGF-β-associated extracellular matrix genes link cancer-associated fibroblasts to immune evasion and immunotherapy failure.** *Nature communications* 2018, **9:**1-10.
46. Turajlic S, Xu H, Litchfield K, Rowan A, Chambers T, Lopez JI, Nicol D, O'Brien T, Larkin J, Horswell S: **Tracking cancer evolution reveals constrained routes to metastases: TRACERx renal.** *Cell* 2018, **173:**581-594. e512.
47. Hakimi AA, Voss MH, Kuo F, Sanchez A, Liu M, Nixon BG, Vuong L, Ostrovnaya I, Chen Y-B, Reuter V: **Transcriptomic profiling of the tumor microenvironment reveals distinct subgroups of clear cell renal cell cancer: data from a randomized phase III trial.** *Cancer discovery* 2019, **9:**510-525.
48. Horn S, Leonardelli S, Sucker A, Schadendorf D, Griewank KG, Paschen A: **Tumor CDKN2A-associated JAK2 loss and susceptibility to immunotherapy resistance.** *JNCI: Journal of the National Cancer Institute* 2018, **110:**677-681.
49. Han G, Yang G, Hao D, Lu Y, Thein K, Simpson BS, Chen J, Sun R, Alhalabi O, Wang R: **9p21 loss confers a cold tumor immune microenvironment and primary resistance to immune checkpoint therapy.** *Nature communications* 2021, **12:**1-19.
50. Laydon DJ, Bangham CR, Asquith B: **Estimating T-cell repertoire diversity: limitations of classical estimators and a new approach.** *Philosophical Transactions of the Royal Society B: Biological Sciences* 2015, **370:**20140291.
51. Riley TP, Keller GL, Smith AR, Davancaze LM, Arbuiso AG, Devlin JR, Baker BM: **Structure based prediction of neoantigen immunogenicity.** *Frontiers in immunology* 2019, **10:**2047.

medRxiv preprint doi: https://doi.org/10.1101/2022.07.11.22277322; this version posted July 13, 2022. The copyright holder for this preprint (which was not certified by peer review) is the author/funder, who has granted medRxiv a license to display the preprint in perpetuity. All rights reserved. No reuse allowed without permission.

52. Bonaventura P, Alcazer V, Mutez V, Tonon L, Martin J, Chuvin N, Michel E, Boulos RE, Estornes Y, Valladeau-Guilemond J: **Identification of shared tumor epitopes from endogenous retroviruses inducing high-avidity cytotoxic T cells for cancer immunotherapy.** *Science Advances* 2022, **8:**eabj3671.
53. Panda A, de Cubas AA, Stein M, Riedlinger G, Kra J, Mayer T, Smith CC, Vincent BG, Serody JS, Beckermann KE: **Endogenous retrovirus expression is associated with response to immune checkpoint blockade in clear cell renal cell carcinoma.** *JCI insight* 2018, **3**.
54. Smith CC, Beckermann KE, Bortone DS, De Cubas AA, Bixby LM, Lee SJ, Panda A, Ganesan S, Bhanot G, Wallen EM: **Endogenous retroviral signatures predict immunotherapy response in clear cell renal cell carcinoma.** *The Journal of clinical investigation* 2019, **128:**4804-4820.
55. Nargund AM, Pham CG, Dong Y, Wang PI, Osmangeyoglu HU, Xie Y, Aras O, Han S, Oyama T, Takeda S: **The SWI/SNF protein PBRM1 restrains VHL-loss-driven clear cell renal cell carcinoma.** *Cell reports* 2017, **18:**2893-2906.
56. Hakimi AA, Attalla K, DiNatale RG, Ostrovnaya I, Flynn J, Blum KA, Ged Y, Hoen D, Kendall SM, Reznik E: **A pan-cancer analysis of PBAF complex mutations and their association with immunotherapy response.** *Nature communications* 2020, **11:**1-11.
57. Liu X-D, Kong W, Peterson CB, McGrail DJ, Hoang A, Zhang X, Lam T, Pilie PG, Zhu H, Beckermann KE: **PBRM1 loss defines a nonimmunogenic tumor phenotype associated with checkpoint inhibitor resistance in renal carcinoma.** *Nature communications* 2020, **11:**1-14.
58. Zhou M, Leung JY, Gessner KH, Hepperla AJ, Simon JM, Davis IJ, Kim WY: **PBRM1 inactivation promotes upregulation of human endogenous retroviruses in a HIF-dependent manner.** *Cancer immunology research* 2022.
59. Zhang Y, Narayanan SP, Mannan R, Raskind G, Wang X, Vats P, Su F, Hosseini N, Cao X, Kumar-Sinha C: **Single-cell analyses of renal cell cancers reveal insights into tumor microenvironment, cell of origin, and therapy response.** *Proceedings of the National Academy of Sciences* 2021, **118**.
60. Zhang AW, McPherson A, Milne K, Kroeger DR, Hamilton PT, Miranda A, Funnell T, Little N, de Souza CP, Laan S: **Interfaces of malignant and immunologic clonal dynamics in ovarian cancer.** *Cell* 2018, **173:**1755-1769. e1722.
61. Levine JH, Simonds EF, Bendall SC, Davis KL, El-ad DA, Tadmor MD, Litvin O, Fienberg HG, Jager A, Zunder ER: **Data-driven phenotypic dissection of AML reveals progenitor-like cells that correlate with prognosis.** *Cell* 2015, **162:**184-197.
62. Xu C, Su Z: **Identification of cell types from single-cell transcriptomes using a novel clustering method.** *Bioinformatics* 2015, **31:**1974-1980.
63. Hegde PS, Chen DS: **Top 10 challenges in cancer immunotherapy.** *Immunity* 2020, **52:**17-35.
64. Motzer RJ, Banchereau R, Hamidi H, Powles T, McDermott D, Atkins MB, Escudier B, Liu L-F, Leng N, Abbas AR: **Molecular subsets in renal cancer determine outcome to checkpoint and angiogenesis blockade.** *Cancer Cell* 2020, **38:**803-817. e804.
65. O'Donnell JS, Teng MW, Smyth MJ: **Cancer immunoediting and resistance to T cell-based immunotherapy.** *Nature reviews Clinical oncology* 2019, **16:**151-167.

medRxiv preprint doi: https://doi.org/10.1101/2022.07.11.22277322; this version posted July 13, 2022. The copyright holder for this preprint (which was not certified by peer review) is the author/funder, who has granted medRxiv a license to display the preprint in perpetuity. All rights reserved. No reuse allowed without permission.

872 **Acknowledgements**

873 **Funding**

874 We thank members of the Chan lab for their suggestions and critical reading of the manuscript.
875 We acknowledge funding sources including NIH R01 CA205426 (T.A.C.), NIH R35 CA232097
876 (T.A.C.), DOD grant KC180165, NIH R01 DE027738 (to L.G.T.M.), the NIH/NCI Cancer Center
877 Support Grant P30 CA008748 (to MSKCC), P30 core grants (to MSKCC), Ludwig institute
878 (A.A.H.), Weiss family fund (A.A.H.), Department of Defense (A.A.H.) and Illumina Inc.

879

880 **Contributions**

881 M.G. performed data analysis and wrote the manuscript with input from all authors. M.G., A.A.H.,
882 T.A.C., and E.R. conceived the study and contributed to data interpretation. F.K., E.R., C.T., V.M.,
883 S.Z., C.Z., and R.M. assisted with analytical methodology development and bioinformatics
884 support. M.L.S., R.V., L.L., T.P., and J.G. contributed to DNA, RNA, and TCR sequencing. R.J.M.,
885 M.I.C., P.R., J.C., L.G.T.M., and M.H.V. cared for patients analyzed in the study. K.A.B. and
886 R.G.N. handled patient samples. R.G.N. collected and analyzed clinical metadata. S.G. and Y.C.
887 analyzed H&E images. All authors read and approved the manuscript.

888

889 **Ethics declarations**

890 **Ethics approval and consent to participate**

891 Informed consent and institutional review board approval were acquired at Memorial Sloan
892 Kettering Cancer Center (MSK).

893 **Consent for publication**

894 Not applicable.

medRxiv preprint doi: https://doi.org/10.1101/2022.07.11.22277322; this version posted July 13, 2022. The copyright holder for this preprint (which was not certified by peer review) is the author/funder, who has granted medRxiv a license to display the preprint in perpetuity. All rights reserved. No reuse allowed without permission.

Competing interests: M.G., R.V., M.L.S., J.G., T.P., R.M., C.Z., S.Z., L.L., are current employees and shareholders of Illumina Inc. T.A.C. and L.G.T.M. are inventors on a patent held by Memorial Sloan Kettering related to the use of TMB in cancer immunotherapy. MSK has licensed the use of TMB for the identification of patients that benefit from immune checkpoint therapy to PGDx. L.G.T.M. reports laboratory research funding from AstraZeneca. T.A.C. is a co-founder of Gritstone Oncology and holds equity. T.A.C. holds equity in An2H. T.A.C. acknowledges grant funding from Bristol-Myers Squibb, AstraZeneca, Illumina, Pfizer, An2H, and Eisai. T.A.C. has served as an advisor for Bristol-Myers Squibb, Illumina, Eisai, and An2H. R.J.M. reports consulting fees from Aveo, Calithera, Eisai, Eli Lilly, EMD Serono, Genentech, Merck, Novartis AG, Pfizer, and Roche, and contracted research to employer MSKCC for Bristol Myers Squibb, Eisai, Exelixis, Genentech, Merck, Pfizer, and Roche. A.A.H. is on the advisory board for Merck. M.H. receives commercial research grants from Bristol-Myers Squibb, Pfizer and Genentech/Roche, honoraria from Novartis, Bristol-Myers Squibb, travel/accommodation from Astra Zeneca, Eisai, Novartis and Takeda, and is a consultant/advisory board member for Alexion Pharmaceuticals, Aveo, Calithera Biosciences, Corvus Pharmaceuticals, Exelixis, Eisai, GlaxoSmithKline, Merck, Natera; Onquality Pharmaceuticals; Novartis and Pfizer. Other authors declare no competing interests.

Figures and Tables

Figure 1. Patient characteristics and study design. a) Multi-regional multi-omics was performed on 29 patients. **b)** In total, 6 out of 29 patients were untreated and the rest were treated with ICI or in combination with TKI. TCRseq of PBMC was performed at 4 time points on therapy for a subset of patients. In addition, pathological review was performed to assign N-TIL (tumors sparsely infiltrated by TILs), S-TIL (tumors dominated by stromal TILs), and ES-TIL (tumors with

medRxiv preprint doi: https://doi.org/10.1101/2022.07.11.22277322; this version posted July 13, 2022. The copyright holder for this preprint (which was not certified by peer review) is the author/funder, who has granted medRxiv a license to display the preprint in perpetuity. All rights reserved. No reuse allowed without permission.

substantial levels of both epithelial and stromal TILs) classes to a subset of patients. **c)** Additionally, scRNAseq data for 6 patients were available from [15].

Figure 2. TME ITH in ccRCC. a) Intra-tumoral heterogeneity of several gene expression signatures across multiple tumor regions. Radar charts show Z-score of each feature normalized across the cohort. Min and max radius for each feature in each panel represent min and max of that feature across the cohort. **b)** For each gene signature, the number of patients who were classified as high or low or a mixture of high and low across tumor regions are shown. Two patients (MR05 and NIVO10) were excluded since WTS data of only one region was available. Also, pre-treatment regions of ICI treated patients were excluded to avoid treatment-related effects in these signatures. **c)** Intra-tumoral heterogeneity of myeloid score observed across multiple regions of tumors of patients in this study.

Figure 3. Landscape of ITH in ccRCC. a) Oncoprint of key ccRCC driver mutations and copy number alterations for all regions of all 29 patients in this cohort. Margin shows comparison between mutation frequency observed in this cohort and TRACERx Renal. **b)** We have performed unsupervised hierarchical clustering of genomic features including patient level presence or absence of a small variant in VHL, PBRM1, SETD2, BAP1 (most commonly mutated genes) as well as loss of heterozygosity in HLA genes as well as 9p (which includes CDKN2A/B) SCNA which are known to affect ICI response. Heatmap shows ITH high vs low classification across data type. Annotation illustrates evolutionary subtypes and treatment status of patients. A patient is annotated as wildtype if all regions are wild type for that alteration. Cases where ITH score could not be calculated due to lack of sufficient number of biopsies are shown in gray pixels. CIN: chromosome instability. **c)** Association between antigen presentation machinery (APM), effector T cell (Teff) and myeloid gene signatures and ITH. Wilcox P, False Discovery Rate (FDR) and

medRxiv preprint doi: https://doi.org/10.1101/2022.07.11.22277322; this version posted July 13, 2022. The copyright holder for this preprint (which was not certified by peer review) is the author/funder, who has granted medRxiv a license to display the preprint in perpetuity. All rights reserved. No reuse allowed without permission.

Linear Mixed Effect (LME) P shown. **d)** Intra-tumoral heterogeneity and myeloid score are associated with CDKN2A/B loss in TCGA KIRC cohort. **e)** ITH low patients show a significantly higher TCR diversity, richness and clone count.

Figure 4. The landscape of heterogeneity of neoantigen depletion. a) Change in the number of non-synonymous binder SNVs (predicted *in silico*) and non-synonymous non-binder SNVs compared to pre-treatment. Reduction in only putative neoantigens illustrates selective pressure and immunoediting. One sample Wilcox test P (compared to zero) is shown. **b)** Clonality of neoantigen depletion. Only strong binders are shown. **c, d)** Immunoediting in an HLA-intact patient NIVO20 through reduced neoantigen expression. NKA/NKB/NKC (shown in RED) are normal adjacent tissues 1cm, 2cm, and 4cm away from the center of the tumor; BX (shown in blue) represents pre-treatment biopsy; RA/RB/RC/RD/RE (shown in green) illustrate 5 tumor regions from the treated tumor sample. **e)** Immunoediting with amino acid resolution. Higher Phenylalanine (F) depletion compared to Glutamic Acid (E) and Arginine (R) suggests immune selection. **f)** Association between putative neoantigen depletion and myeloid activation across all regions of patients where pre-treatment WES data was available (n = 16 patients). **g)** Association between the fraction of expressed putative neoantigens depleted and immune signatures. In (**g**) correlations are calculated across different regions of the same patient, for all patients with >3 treated as well as pre-treatment RNA samples were available (n = 7 patients). **h, i)** HERVs are enriched in tumors compared to normal samples and are associated with treatment. **j)** HERV depletion association with myeloid signature. **k)** Circos plot (left) illustrates the fraction of shared T cell clonotypes between tissue and different time points on therapy. Ribbons connecting different regions of the tumor are scaled based on clonotype overlap. (right) clonotype tracking of dominant untreated T cell clones in treated regions of patient NIVO20. The color of each ribbon shows different T cell clones, and the width is scaled corresponding to the frequency of that clone.

medRxiv preprint doi: https://doi.org/10.1101/2022.07.11.22277322; this version posted July 13, 2022. The copyright holder for this preprint (which was not certified by peer review) is the author/funder, who has granted medRxiv a license to display the preprint in perpetuity. All rights reserved. No reuse allowed without permission.

969 Tissue data consists of 5 tumor regions after treatment (RA/RB/RC/RD/RE), one single normal
970 adjacent (NKC), and one tumor region pre-treatment (BX). Likewise, PBMC data points on
971 treatment are NIVO20-68, -54, -40, -12. **l, m)** TCR diversity is negatively associated with
972 neoantigen depletion and HLA LOH.

973

974 **Figure 5. Branch evolution demonstrates immune evasion. a)** Evolutionary tree illustrates
975 tumors can exploit concurrent HLA LOH and CDKN2A/B loss to escape immune surveillance. **b)**
976 Co-occurrence of HLA LOH and CDKN2A/B can be seen both across regions and patients. **c)**
977 Differential immune response to ICI therapy in patients with CDKN2A/B loss or HLA LOH or
978 belonging to ITH high subtype. **d)** Regions of tumor associated with immune escape depict a
979 distinct pathology where colocalization of TILs and stroma can be observed.

980

981 **Figure 6. Immunoediting correlates with stroma and myeloid signatures. a)** WGCNA
982 identifies gene expression modules associated with inflammation ("JAVELIN-like"), angiogenesis,
983 and Immune Escape. Gene dendrogram was first generated and then modules were extracted
984 using dynamic tree cutting (top). Modules were annotated by comparing the correlation between
985 the module eigengenes and previously known gene signatures describing different phenotypes
986 (bottom). **b)** Modules 7 (black), 4 (salmon), and 16 (magenta) are associated with previously
987 described signatures, JAVELIN, angiogenesis and myeloid/stroma. **c)** scRNAseq demonstrates
988 the cell type enrichment of Immune Escape signature in ccRCC patients. Different colors
989 represent different cell types inferred from scRNAseq data. UMAP plot illustrates single cells
990 collected from all 6 patients including treated and untreated patients. Computational extracted
991 clusters were annotated as previously described [15] **d, e)** Association between ITH groups,
992 Immune Escape signature and N/S/ES pathologies. **f)** These regions demonstrate an elevated

medRxiv preprint doi: https://doi.org/10.1101/2022.07.11.22277322; this version posted July 13, 2022. The copyright holder for this preprint (which was not certified by peer review) is the author/funder, who has granted medRxiv a license to display the preprint in perpetuity. All rights reserved. No reuse allowed without permission.

Immune Escape gene signature in NIVO21. RA, RB, RC, RD, and RE denote different regions of a tumor sample.

Figure 7. Association between immune escape and clinical outcome to checkpoint blockade. Survival analysis shows the association between gene signatures obtained in this study and clinical outcome of different independent retrospective trials. **a)** Immune Escape and JAVELIN-like signatures are associated with PFS in patients treated Avelumab plus Axitinib in JAVELIN Renal 101 cohort. **b)** Immune Escape signature, but not the JAVELIN-like signature, correlates with the response to Atezolizumab plus Bevacizumab in IMmotion151 but not JAVELIN signature. **c)** Immune Escape signature, but not the JAVELIN-like signature, correlates with the efficacy of anti-PD1-treament in CheckMate 009, 010, 025.

Figure 8. A hypothetical model for spatiotemporal evolution of ccRCC links ITH to immune escape and adverse TME. Cancer cell death, potentially by cytotoxic killing, early in tumor evolution selects for tumor clones with HLA LOH and/or CDKN2A/B loss. This promotes the evolution of a TME depleted of antigen-specific T cells and enriched for myeloid cells.

Supplementary Figure Legends

Fig. S1. Validation of TME associated gene signatures using IF. Myeloid signature correlates with CD11b/CD68 markers. CD31 endothelial and CD8 T cell markers are correlated with Angiogenesis and JAVELIN signatures.

Fig. S2. ccRCC evolutionary subtypes and their association with angiogenic TME score.

Fig. S3. Clonotype overlap analysis. a) Hierarchical clustering of TCR clonotypes across different regions of patients where tissue TCRseq data was available. **B)** Rarefration analysis of

medRxiv preprint doi: https://doi.org/10.1101/2022.07.11.22277322; this version posted July 13, 2022. The copyright holder for this preprint (which was not certified by peer review) is the author/funder, who has granted medRxiv a license to display the preprint in perpetuity. All rights reserved. No reuse allowed without permission.

ITH high vs ITH low patients **c)** Circos plot illustrates the fraction of shared T cell clonotypes between tissue and different time points on therapy. Ribbons connecting different regions of the tumor are scaled based on clonotype overlap. Labels show patient ID followed by time to nephrectomy (e.g., NIVO09-7: patient NIVO09 at 7 days to nephrectomy) **d)** Number of CDR3 clone counts shown for all samples where TCR seq was performed.

Fig. S4. Boxplots show total and change compared to pre-treatment (when sample was available) for mutational count, and neoantigen count across different regions of all patients. Count change is shown only for 16 patients whose pre-treatment WES data was available.

Fig. S5. Association between neoantigen loss and myeloid signature. a) No association between TMB and tumor purity (FACETS) was observed **b)** Association between total number of neoantigens depleted and myeloid signature. **c)** The fraction of mutations or neoantigens depleted is not correlated with tumor purity for samples with tumor purity larger than 0.3; however, the association between myeloid signature and neoantigen depletion remains strong even after excluding samples with low purity. **d)** Association between immune elimination and escape with myeloid signature.

Fig. S6. Comparison between SNPs neoantigen depletion and INDEL depletion.

Fig. S7. Treatment impact of HERV association with TME. a) Association between HERV expression and immune signatures. **b)** PBRM1 mutations are associated with elevated HERV expression**. c)** Association between ClearCode34 classes and HERV expression. **d)** Association between ClearCode34 classes and neoantigen depletion.

Fig. S8. Association between immune escape signature and treatment.

medRxiv preprint doi: https://doi.org/10.1101/2022.07.11.22277322; this version posted July 13, 2022. The copyright holder for this preprint (which was not certified by peer review) is the author/funder, who has granted medRxiv a license to display the preprint in perpetuity. All rights reserved. No reuse allowed without permission.

Fig. S9. Validation of escape signature in independent cohorts (IMmotion151). a) Escape signature is associated with improved survival in patients treated with ICI but not sunitinib**. b)** Escape signature is associated with CDKN2A/B alteration in Immotion151.

Fig. S10. Relationship between escape gene signature and treatment outcome in different clinical trials. HRs are calculated for each threshold for ICI or ICI in combination with TKI arms in JAVELIN Renal 101, IMmotion151, and CheckMate 009, 010, 025.

Fig. S11. Refinement of immune escape gene signature. a) 85 genes immune escape gene signature is strongly associated with response to Avelumab plus Axitinib in JAVELIN Renal 101 trial. **b)** Pairwise spearman correlation between 85 genes in module 16 (immune escape). **c)** Refinement of 85 genes into 12 genes with the highest pairwise spearman correlation.

Supplementary Materials

Supplementary Tables

Table S1: Data availability.

Table S2: Patient characteristics and relevant clinical data.

Table S3: WTS related gene signatures.

Table S4: ITH classification.

Figure 1

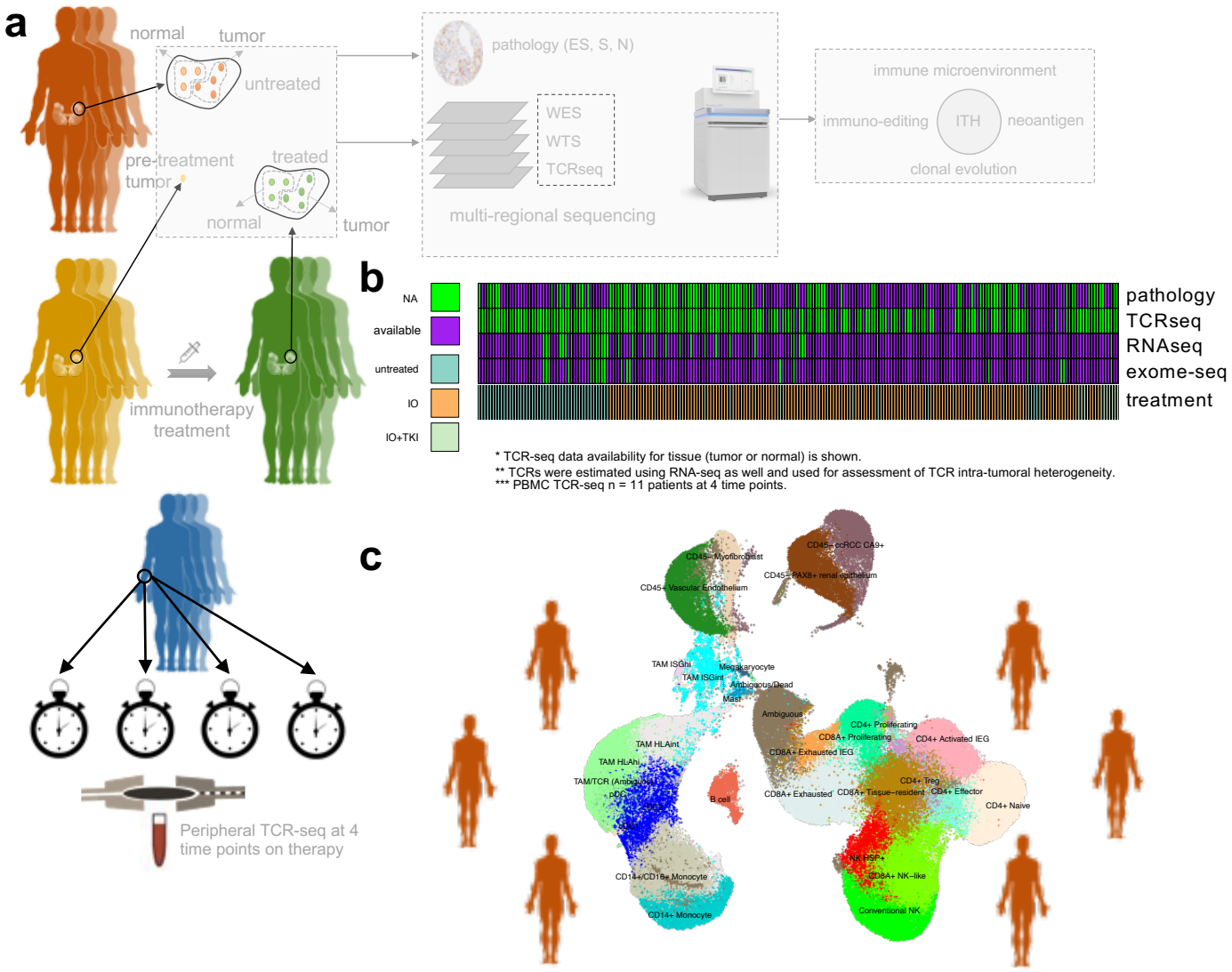
a
normal
tumor
untreated
pre-treatment tumor
treated
normal
tumor
immunotherapy treatment
pathology (ES, S, N)
WES
WTS
TCRseq
multi-regional sequencing
immune microenvironment
immuno-editing
ITH
neoantigen
clonal evolution
b
NA
available
untreated
IO
IO+TKI
pathology
TCRseq
RNAseq
exome-seq
treatment
* TCR-seq data availability for tissue (tumor or normal) is shown.
** TCRs were estimated using RNA-seq as well and used for assessment of TCR intra-tumoral heterogeneity.
*** PBMC TCR-seq n = 11 patients at 4 time points.
c
Peripheral TCR-seq at 4 time points on therapy
CD45− Myofibroblast
CD45− ccRCC CA9+
CD45− Vascular Endothelium
CD45− PAX8+ renal epithelium
TAM ISGhi
Megakaryocyte
TAM ISGint
Ambiguous/Dead
Mast
Ambiguous
CD4+ Proliferating
CD8A+ Proliferating
CD4+ Activated IEG
TAM HLAint
CD8A+ Exhausted IEG
TAM HLAhi
TAM/TCR (Ambiguous)
pDC
B cell
CD4+ Treg
CD8A+ Exhausted
CD8A+ Tissue−resident
CD4+ Effector
CD4+ Naive
cDC2
cDC1
NK HSP+
CD8A+ NK−like
CD14+/CD16+ Monocyte
CD14+ Monocyte
Conventional NK

Figure 2

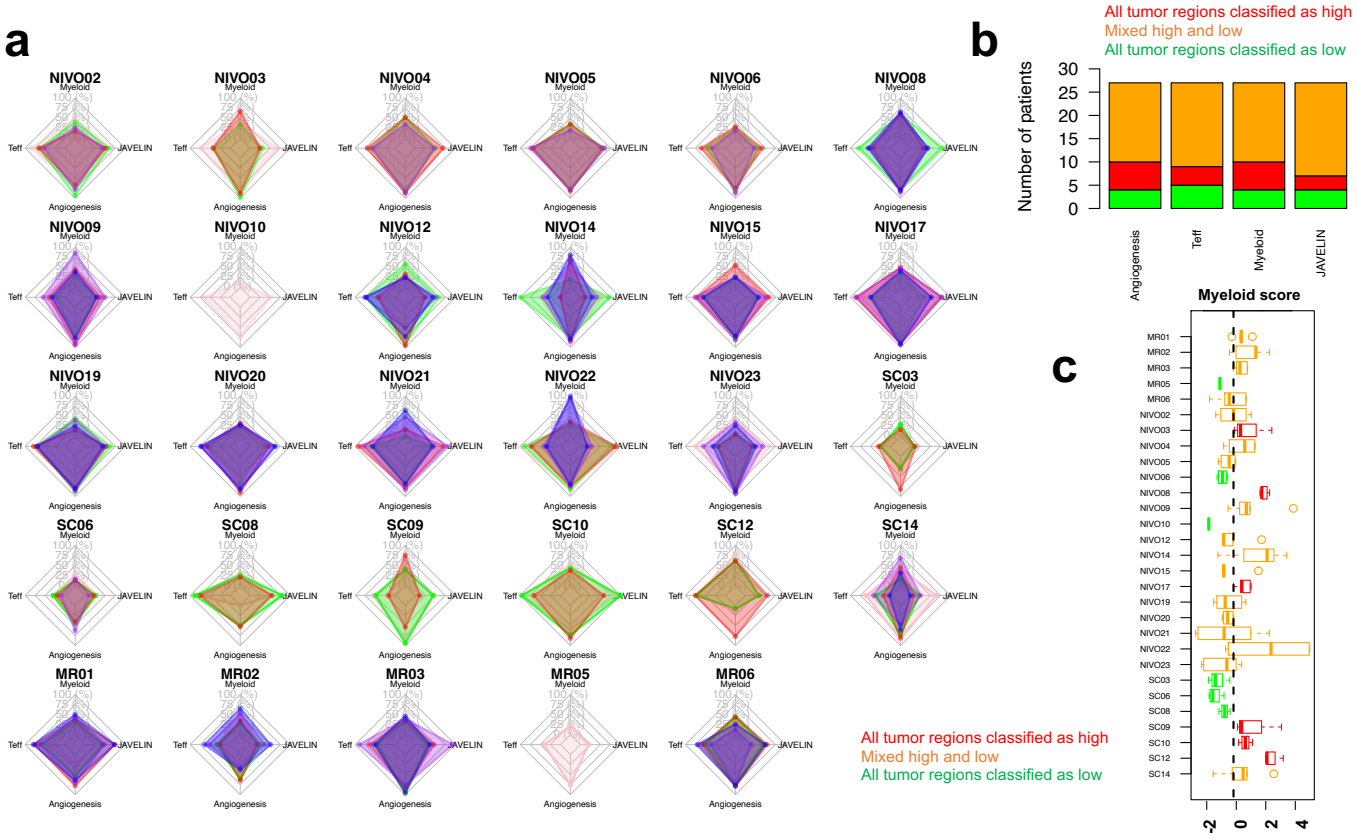
a
NIVO02
NIVO03
NIVO04
NIVO05
NIVO06
NIVO08
NIVO09
NIVO10
NIVO12
NIVO14
NIVO15
NIVO17
NIVO19
NIVO20
NIVO21
NIVO22
NIVO23
SC03
SC06
SC08
SC09
SC10
SC12
SC14
MR01
MR02
MR03
MR05
MR06
Myeloid
Teff
JAVELIN
Angiogenesis
All tumor regions classified as high
Mixed high and low
All tumor regions classified as low
b
Number of patients
Angiogenesis
Teff
Myeloid
JAVELIN
c
Myeloid score

Figure 3

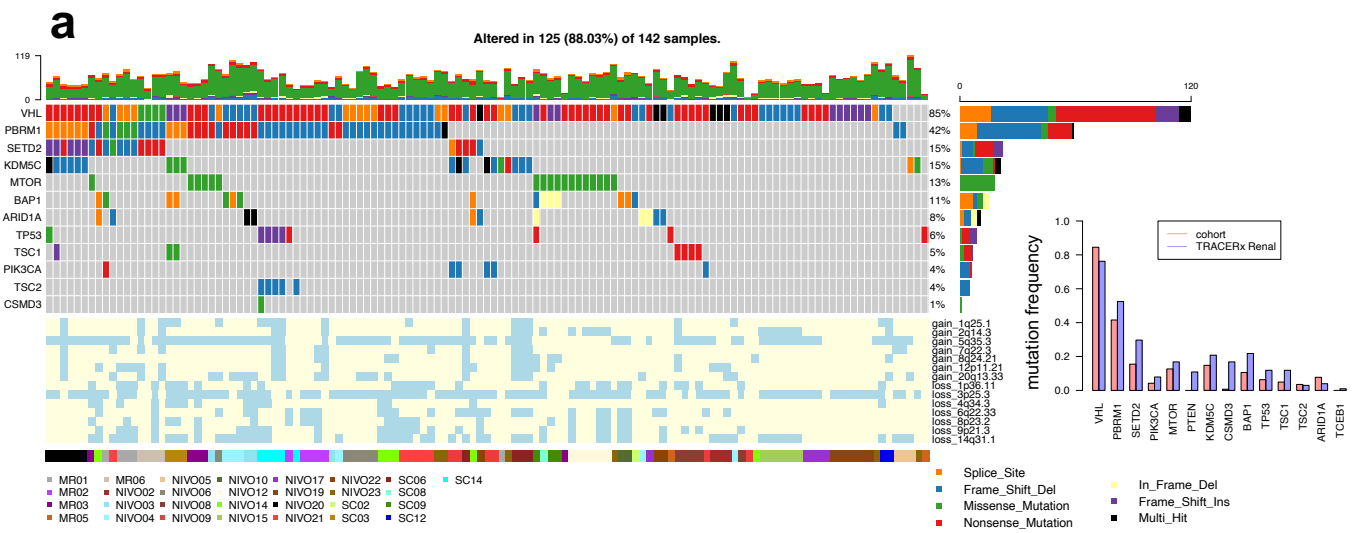
a
Altered in 125 (88.03%) of 142 samples.
VHL
PBRM1
SETD2
KDM5C
MTOR
BAP1
ARID1A
TP53
TSC1
PIK3CA
TSC2
CSMD3
85%
42%
15%
15%
13%
11%
8%
6%
5%
4%
4%
1%
mutation frequency
cohort
TRACERx Renal
gain_1q25.1
gain_2q14.3
gain_5q35.3
gain_7q22.3
gain_8q24.21
gain_12p11.21
gain_20q13.33
loss_1p36.11
loss_3p25.3
loss_4q34.3
loss_8q22.33
loss_8p23.2
loss_9p21.3
loss_14q31.1
MR01
MR02
MR03
MR05
MR06
NIVO02
NIVO03
NIVO04
NIVO05
NIVO06
NIVO08
NIVO09
NIVO10
NIVO12
NIVO14
NIVO15
NIVO17
NIVO19
NIVO20
NIVO21
NIVO22
NIVO23
SC02
SC03
SC06
SC08
SC09
SC12
SC14
Splice_Site
Frame_Shift_Del
Missense_Mutation
Nonsense_Mutation
In_Frame_Del
Frame_Shift_Ins
Multi_Hit

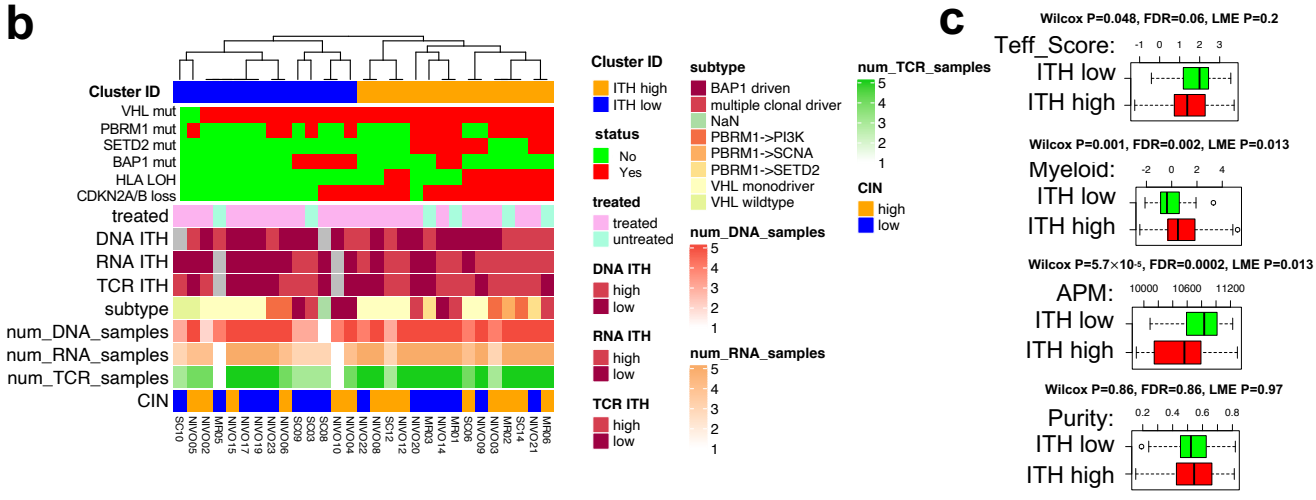
b
Cluster ID
VHL mut
PBRM1 mut
SETD2 mut
BAP1 mut
HLA LOH
CDKN2A/B loss
treated
DNA ITH
RNA ITH
TCR ITH
subtype
num_DNA_samples
num_RNA_samples
num_TCR_samples
CIN
ITH high
ITH low
status
No
Yes
treated
untreated
BAP1 driven
multiple clonal driver
NaN
PBRM1->PI3K
PBRM1->SCNA
PBRM1->SETD2
VHL monodriver
VHL wildtype
high
low
c
Wilcox P=0.048, FDR=0.06, LME P=0.2
Teff_Score:
Wilcox P=0.001, FDR=0.002, LME P=0.013
Myeloid:
Wilcox P=5.7×10-5, FDR=0.0002, LME P=0.013
APM:
Wilcox P=0.86, FDR=0.86, LME P=0.97
Purity:

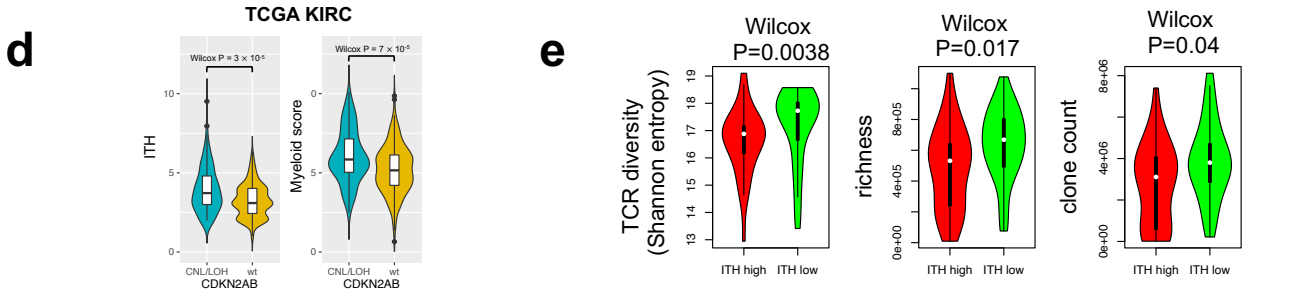
d
TCGA KIRC
Wilcox P = 3 × 10-5
Wilcox P = 7 × 10-5
ITH
Myeloid score
CNL/LOH
wt
CDKN2AB
e
Wilcox P=0.0038
Wilcox P=0.017
Wilcox P=0.04
TCR diversity (Shannon entropy)
richness
clone count
ITH high
ITH low

Figure 4

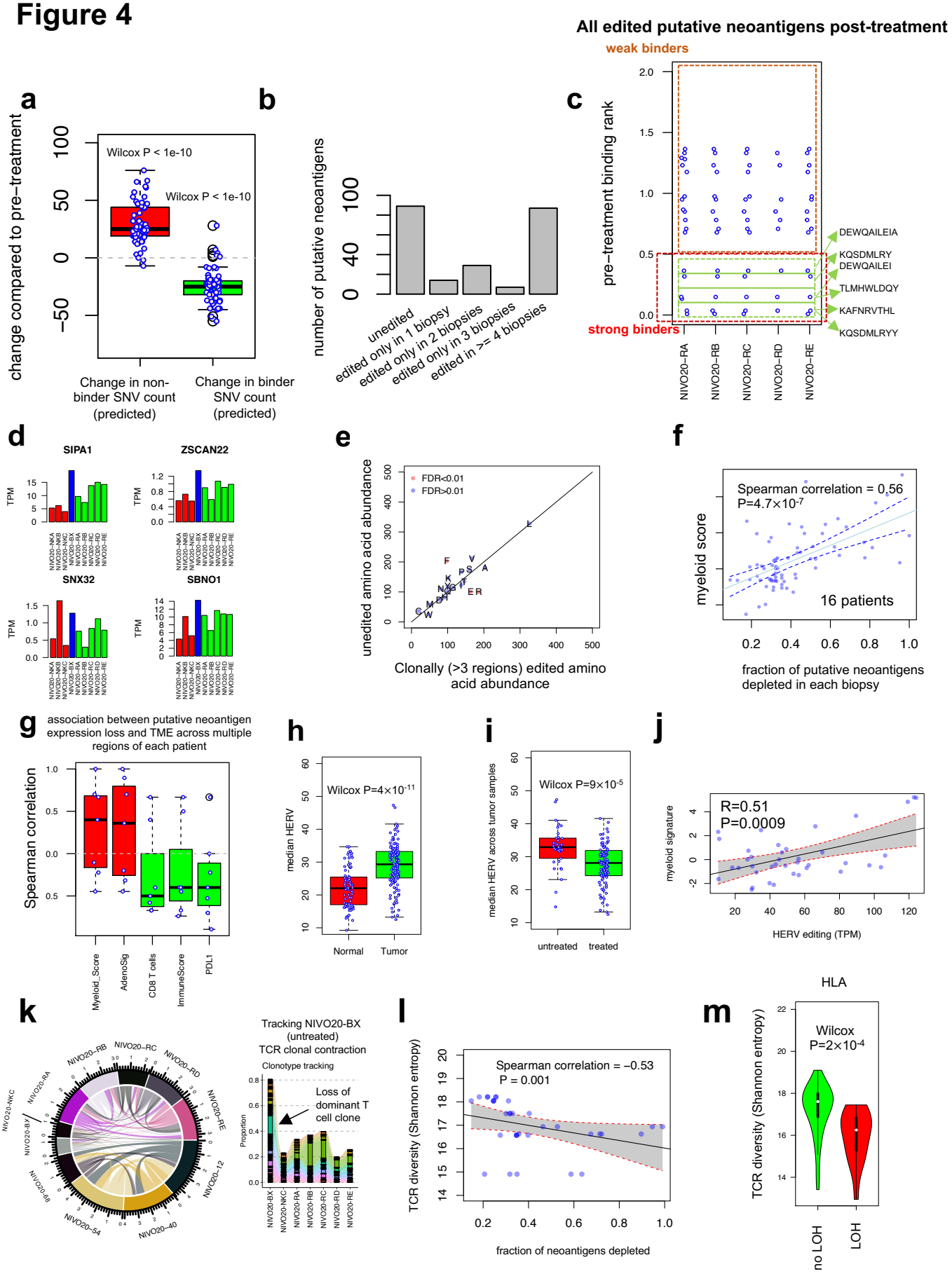
All edited putative neoantigens post-treatment
weak binders
strong binders
a
b
c
d
e
f
g
h
i
j
k
l
m
change compared to pre−treatment
Wilcox P < 1e-10
Wilcox P < 1e-10
Change in non-binder SNV count (predicted)
Change in binder SNV count (predicted)
number of putative neoantigens
unedited
edited only in 1 biopsy
edited only in 2 biopsies
edited only in 3 biopsies
edited in >= 4 biopsies
pre−treatment binding rank
DEWQAILEIA
KQSDMLRY
DEWQAILEI
TLMHWLDQY
KAFNRVTHL
KQSDMLRYY
NIVO20−RA
NIVO20−RB
NIVO20−RC
NIVO20−RD
NIVO20−RE
SIPA1
ZSCAN22
SNX32
SBNO1
TPM
FDR<0.01
FDR>0.01
unedited amino acid abundance
Clonally (>3 regions) edited amino acid abundance
Spearman correlation = 0.56
P=4.7×10-7
16 patients
myeloid score
fraction of putative neoantigens depleted in each biopsy
association between putative neoantigen expression loss and TME across multiple regions of each patient
Spearman correlation
Myeloid_Score
AdenoSig
CD8 T cells
ImmuneScore
PDL1
Wilcox P=4×10-11
median HERV
Normal
Tumor
Wilcox P=9×10-5
median HERV across tumor samples
untreated
treated
R=0.51
P=0.0009
myeloid signature
HERV editing (TPM)
Tracking NIVO20-BX (untreated)
TCR clonal contraction
Clonotype tracking
Loss of dominant T cell clone
Proportion
Spearman correlation = −0.53
P = 0.001
TCR diversity (Shannon entropy)
fraction of neoantigens depleted
HLA
Wilcox P=2×10-4
no LOH
LOH

Figure 5

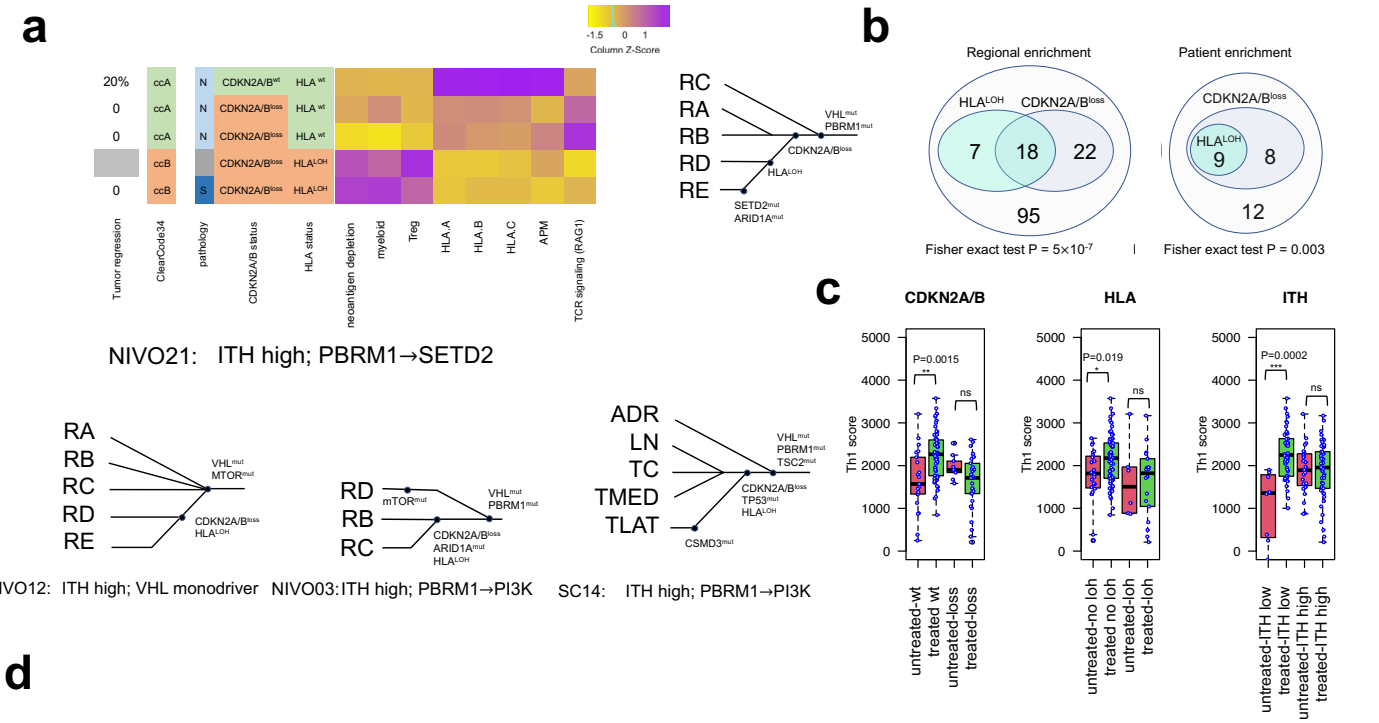
a
Column Z-Score
-1.5 0 1
Tumor regression
ClearCode34
pathology
CDKN2A/B status
HLA status
neoantigen depletion
myeloid
Treg
HLA.A
HLA.B
HLA.C
APM
TCR signaling (RAG1)
RC
RA
RB
RD
RE
VHL mut PBRM1 mut
CDKN2A/B loss
HLA LOH
SETD2 mut ARID1A mut
b
Regional enrichment
Patient enrichment
HLA LOH
CDKN2A/B loss
7
18
22
95
9
8
12
Fisher exact test P = 5×10-7
Fisher exact test P = 0.003
c
CDKN2A/B
HLA
ITH
Th1 score
P=0.0015
P=0.019
P=0.0002
ns
untreated-wt
treated wt
untreated-loss
treated-loss
untreated-no loh
treated no loh
untreated-loh
treated-loh
untreated-ITH low
treated-ITH low
untreated-ITH high
treated-ITH high
NIVO21: ITH high; PBRM1→SETD2
RA
RB
RC
RD
RE
VHL mut MTOR mut
CDKN2A/B loss HLA LOH
NIVO12: ITH high; VHL monodriver
RD
RB
RC
mTOR mut
VHL mut PBRM1 mut
CDKN2A/B loss ARID1A mut HLA LOH
NIVO03:ITH high; PBRM1→PI3K
ADR
LN
TC
TMED
TLAT
VHL mut PBRM1 mut TSC2 mut
CDKN2A/B loss TP53 mut HLA LOH
CSMD3 mut
SC14: ITH high; PBRM1→PI3K

d

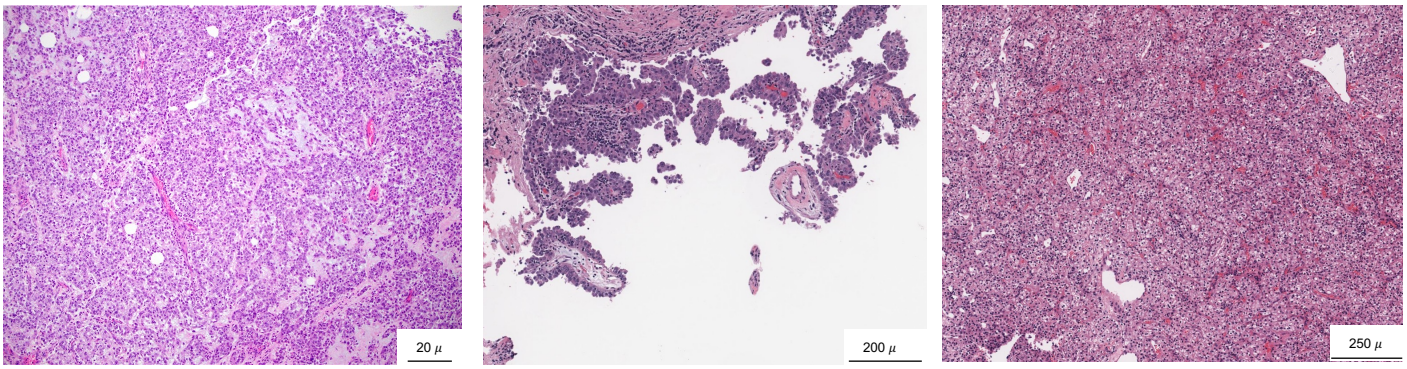
20 μ
200 μ
250 μ
N
S
ES

Figure 6

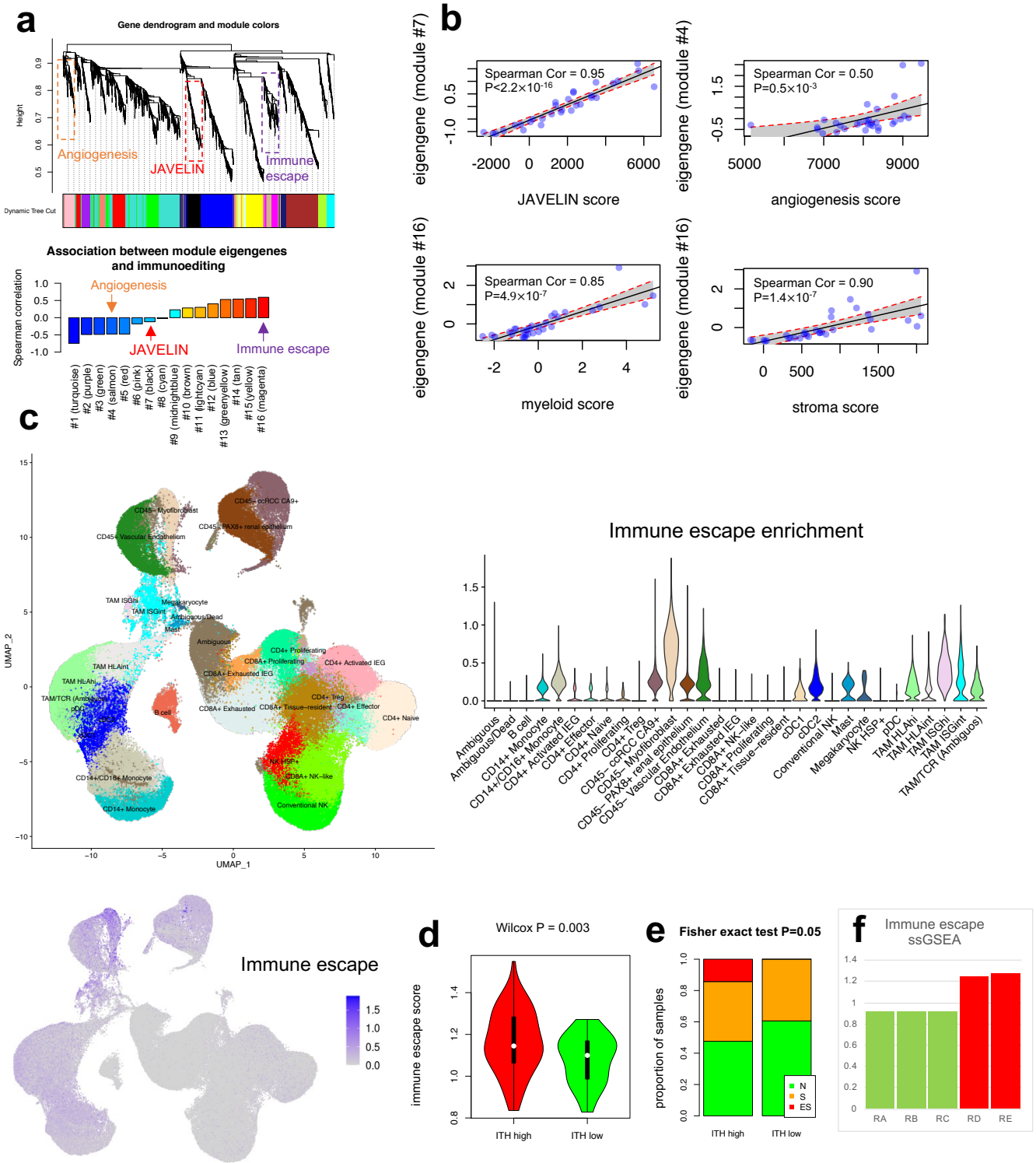
a
Gene dendrogram and module colors
Height
Dynamic Tree Cut
Angiogenesis
JAVELIN
Immune escape
Association between module eigengenes and immunoediting
Spearman correlation
Angiogenesis
JAVELIN
Immune escape
#1 (turquoise)
#2 (purple)
#3 (green)
#4 (salmon)
#5 (red)
#6 (pink)
#7 (black)
#8 (cyan)
#9 (midnightblue)
#10 (brown)
#11 (lightcyan)
#12 (blue)
#13 (greenyellow)
#14 (tan)
#15 (yellow)
#16 (magenta)
b
eigengene (module #7)
Spearman Cor = 0.95
P<2.2×10-16
JAVELIN score
eigengene (module #4)
Spearman Cor = 0.50
P=0.5×10-3
angiogenesis score
eigengene (module #16)
Spearman Cor = 0.85
P=4.9×10-7
myeloid score
eigengene (module #16)
Spearman Cor = 0.90
P=1.4×10-7
stroma score
c
UMAP_1
UMAP_2
CD45− Myofibroblast
CD45+ Vascular Endothelium
CD45− ccRCC CA9+
CD45− PAX8+ renal epithelium
TAM ISGhi
TAM ISGint
Megakaryocyte
Ambiguous/Dead
Mast
Ambiguous
CD4+ Proliferating
CD8A+ Proliferating
CD4+ Activated IEG
CD8A+ Exhausted IEG
TAM HLAint
TAM HLAhi
TAM/TCR (Ambiguous)
pDC
cDC2
B cell
CD8A+ Exhausted
CD8A+ Tissue−resident
CD4+ Treg
CD4+ Effector
CD4+ Naive
NK HSP+
CD8A+ NK−like
CD14+/CD16+ Monocyte
CD14+ Monocyte
Conventional NK
Immune escape enrichment
Ambiguous
Ambiguous/Dead
B cell
CD14+ Monocyte
CD14+/CD16+ Monocyte
CD4+ Activated IEG
CD4+ Effector
CD4+ Naive
CD4+ Proliferating
CD4+ Treg
CD45− ccRCC CA9+
CD45− Myofibroblast
PAX8+ renal epithelium
CD45− Vascular Endothelium
CD8A+ Exhausted
CD8A+ Exhausted IEG
CD8A+ NK−like
CD8A+ Proliferating
CD8A+ Tissue−resident
cDC1
cDC2
Conventional NK
Mast
Megakaryocyte
NK HSP+
pDC
TAM HLAhi
TAM HLAint
TAM ISGhi
TAM ISGint
TAM/TCR (Ambiguous)
Immune escape
d
Wilcox P = 0.003
immune escape score
ITH high
ITH low
e
Fisher exact test P=0.05
proportion of samples
N
S
ES
ITH high
ITH low
f
Immune escape ssGSEA
RA
RB
RC
RD
RE

Figure 7

a

RJ Motzer *et al.* (JAVELIN Renal 101) n=354

Avelumab plus Axitinib

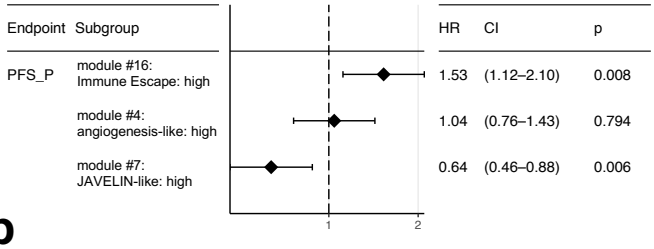

RJ Motzer *et al.* (JAVELIN Renal 101) n=372

Sunitinib

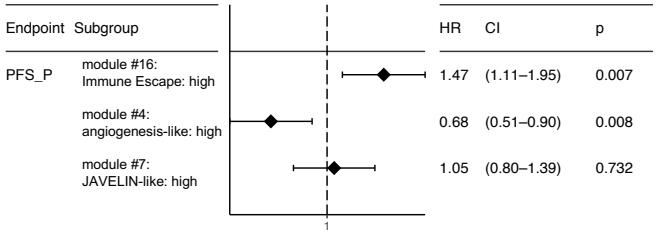

b

RJ Motzer *et al.* (IMmotion151) n=407

Atezolizumab plus Bevacizumab

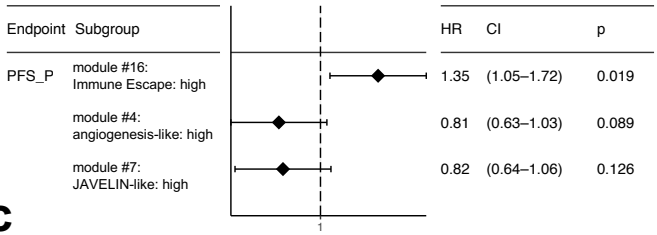

RJ Motzer *et al.* (IMmotion151) n=416

Sunitinib

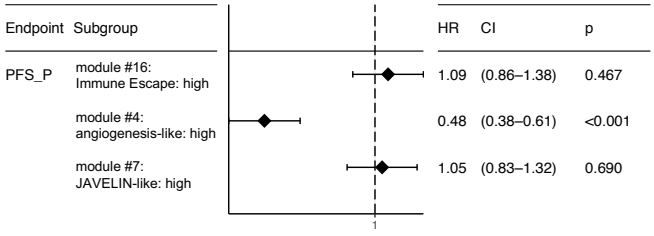

c

DA Braun *et al.* (CheckMate 009, 010, 025) n=181

Anti-PD1-treatment

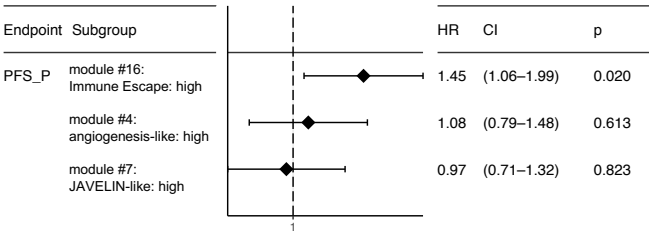

DA Braun *et al.* (CheckMate 009, 010, 025) n=130

mTOR inhibition

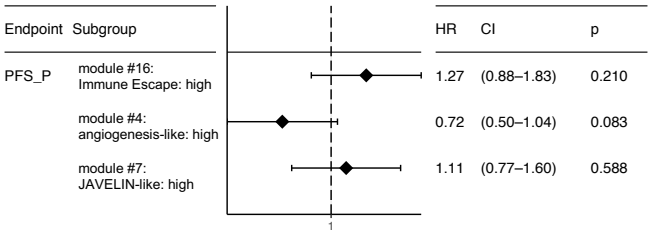

Figure 8

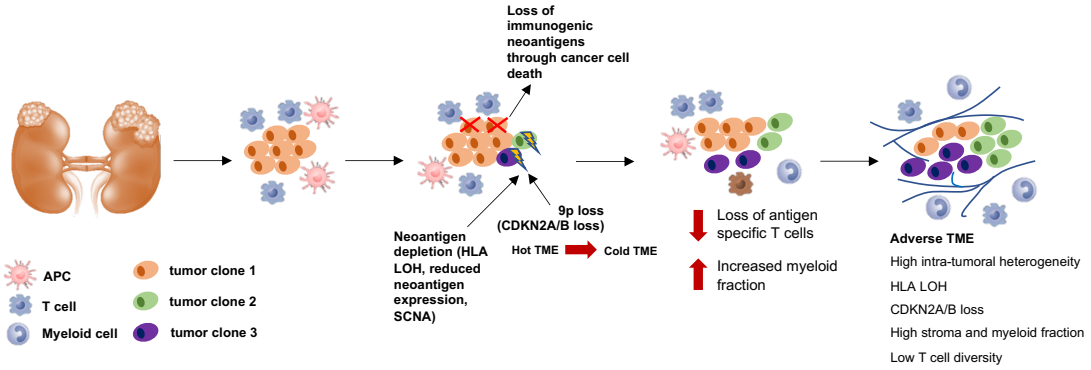
Loss of immunogenic neoantigens through cancer cell death
9p loss (CDKN2A/B loss)
Neoantigen depletion (HLA LOH, reduced neoantigen expression, SCNA)
Hot TME
Cold TME
Loss of antigen specific T cells
Increased myeloid fraction
Adverse TME
High intra-tumoral heterogeneity
HLA LOH
CDKN2A/B loss
High stroma and myeloid fraction
Low T cell diversity
APC
T cell
Myeloid cell
tumor clone 1
tumor clone 2
tumor clone 3

Extended Data Fig. 1

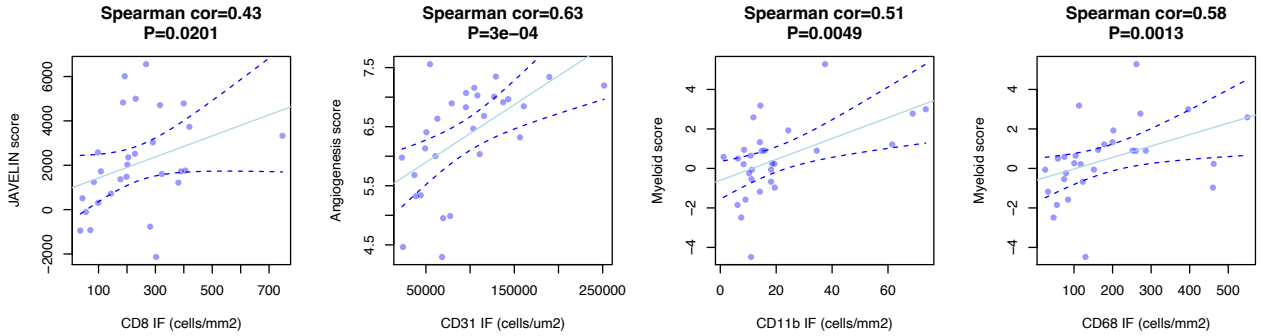

Extended Data Fig. 2

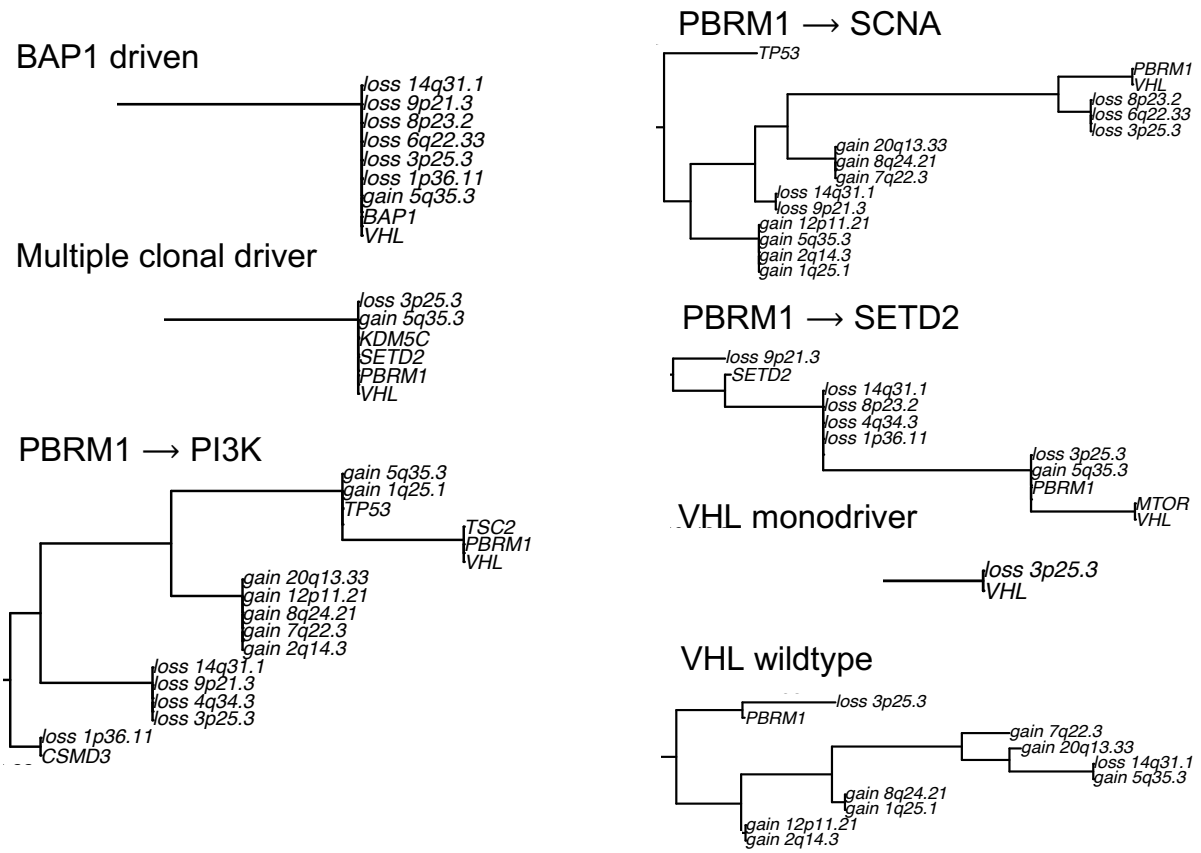

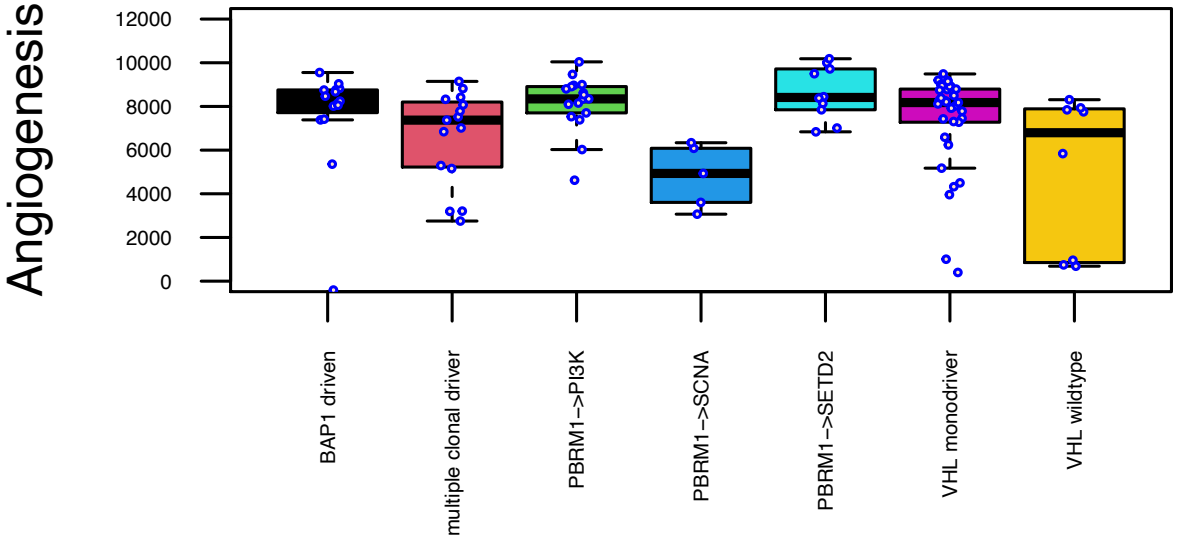

Extended Data Fig. 3

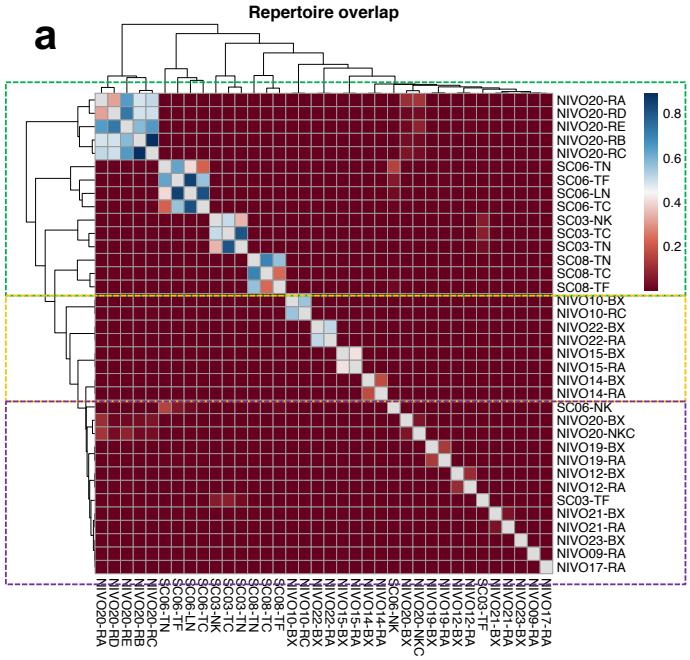

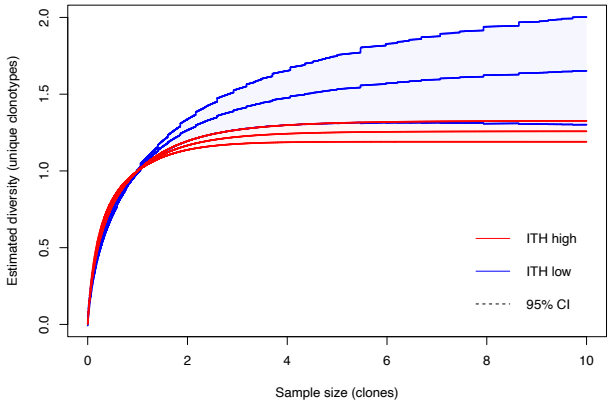

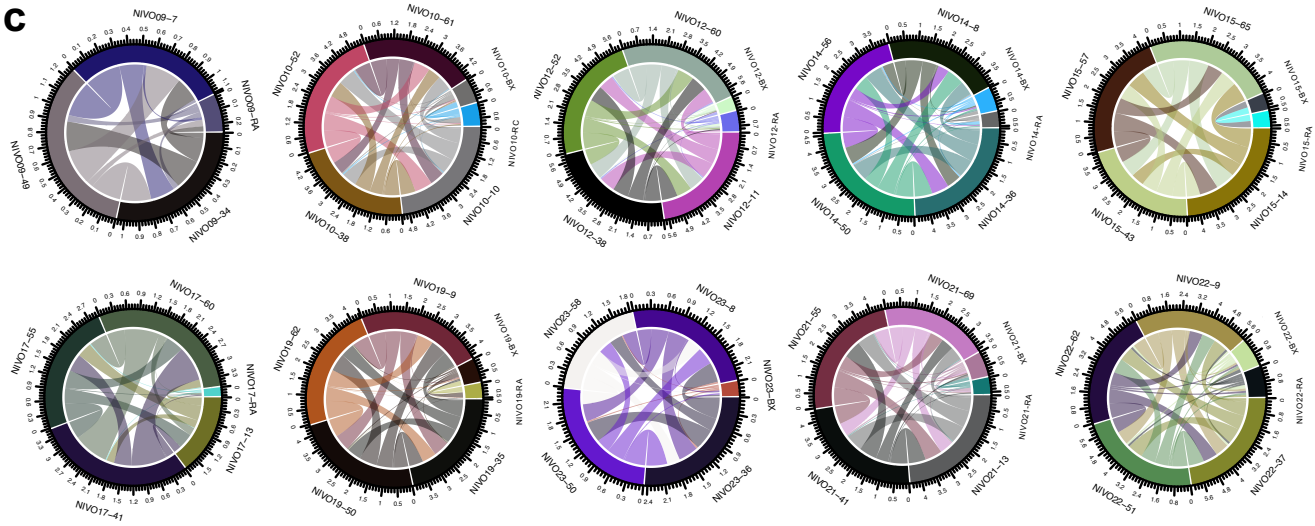

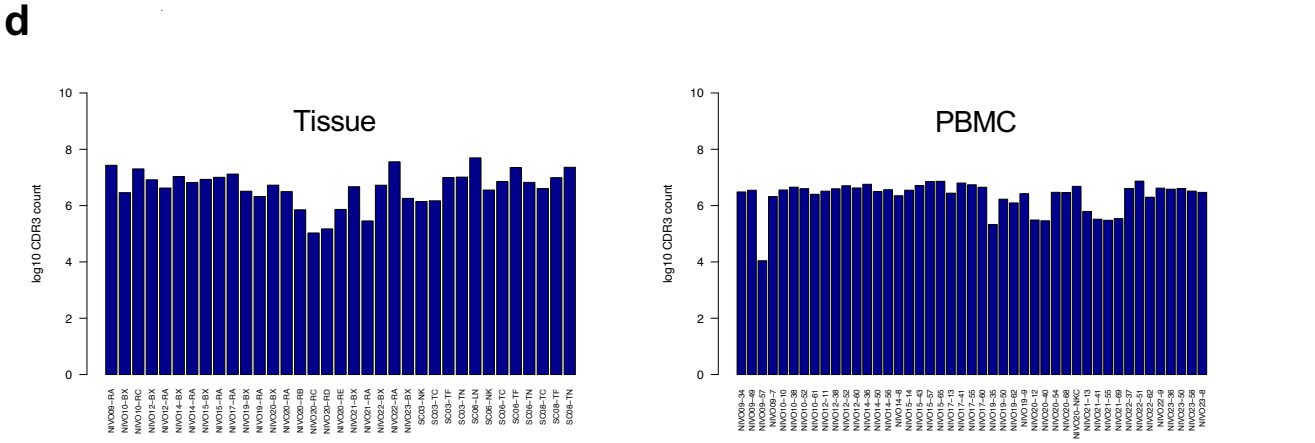

Extended Data Fig. 4

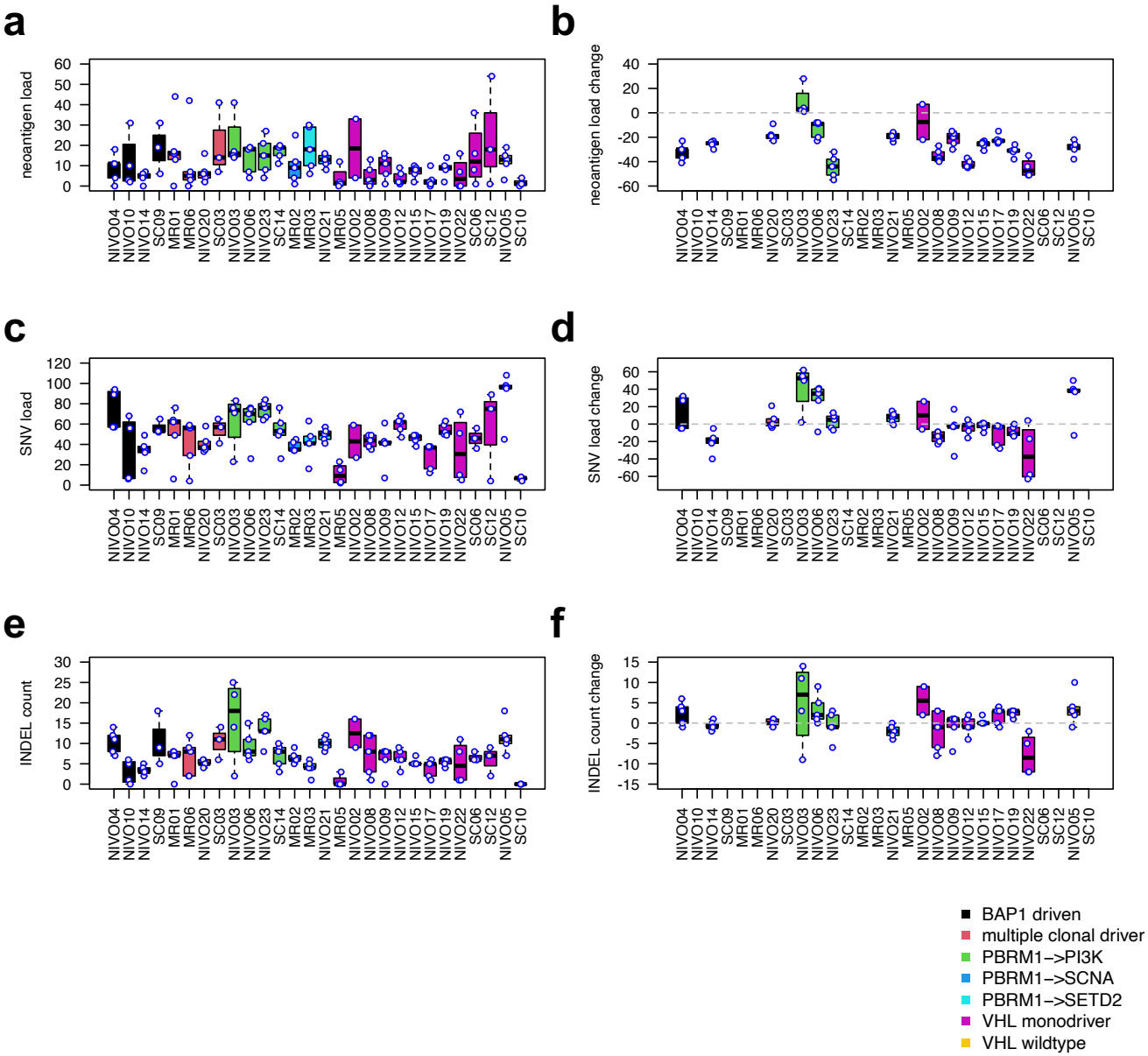

Extended Data Fig. 5

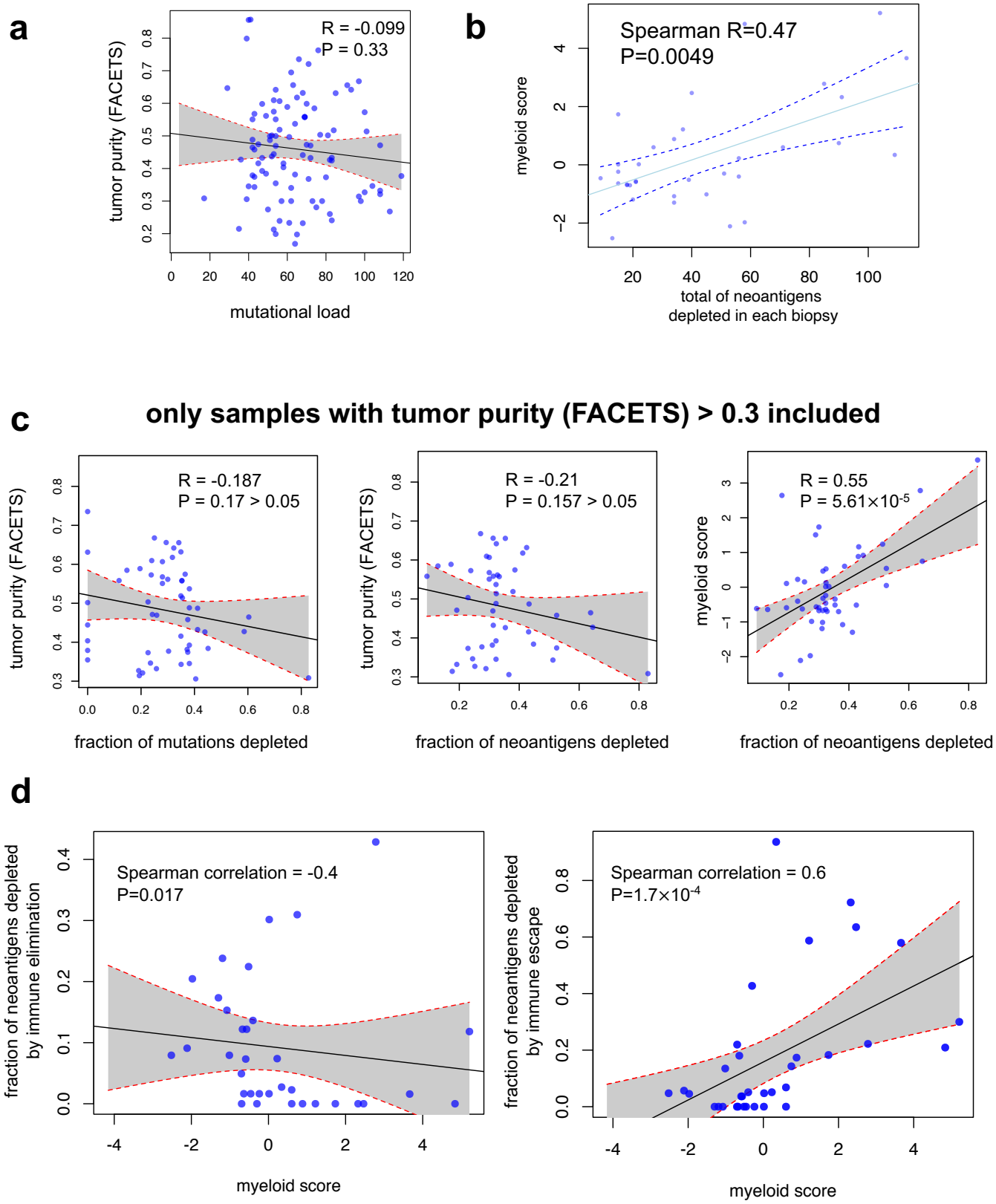

Extended Data Fig. 6

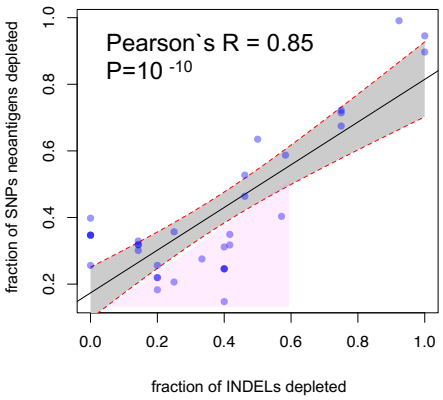

Extended Data Fig. 7

a

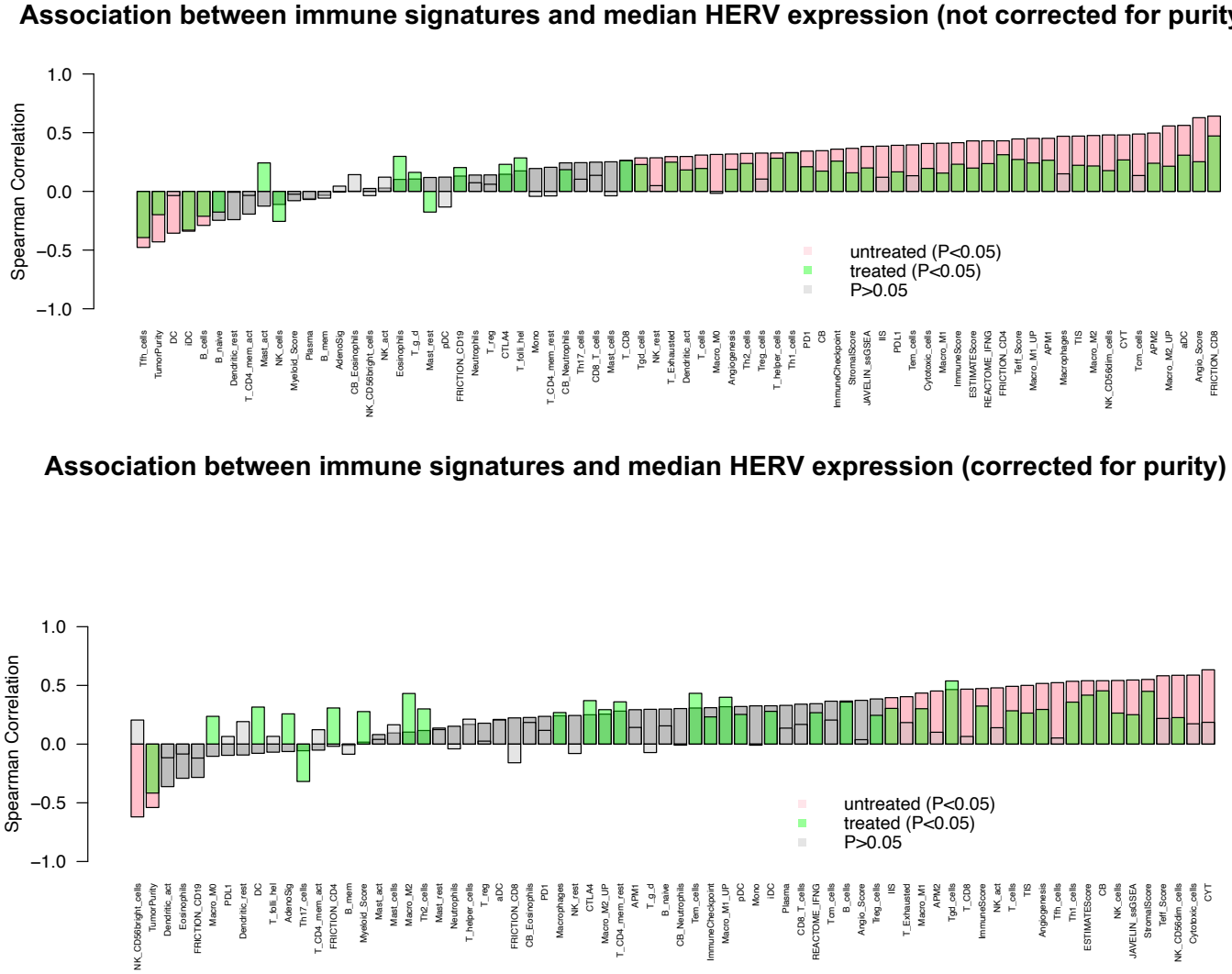

b

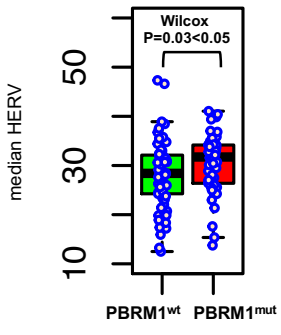

c

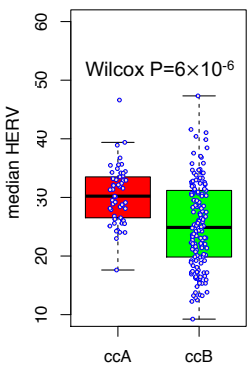

d

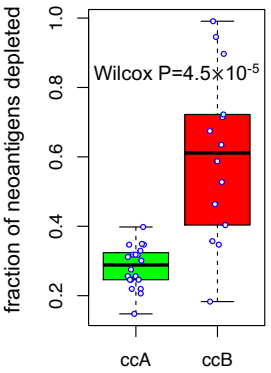

Extended Data Fig. 8

a

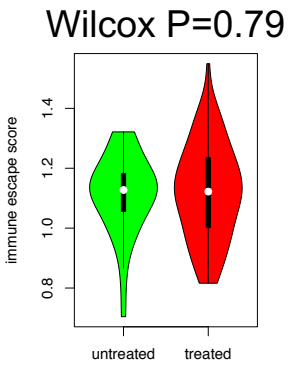

Extended Data Fig. 9

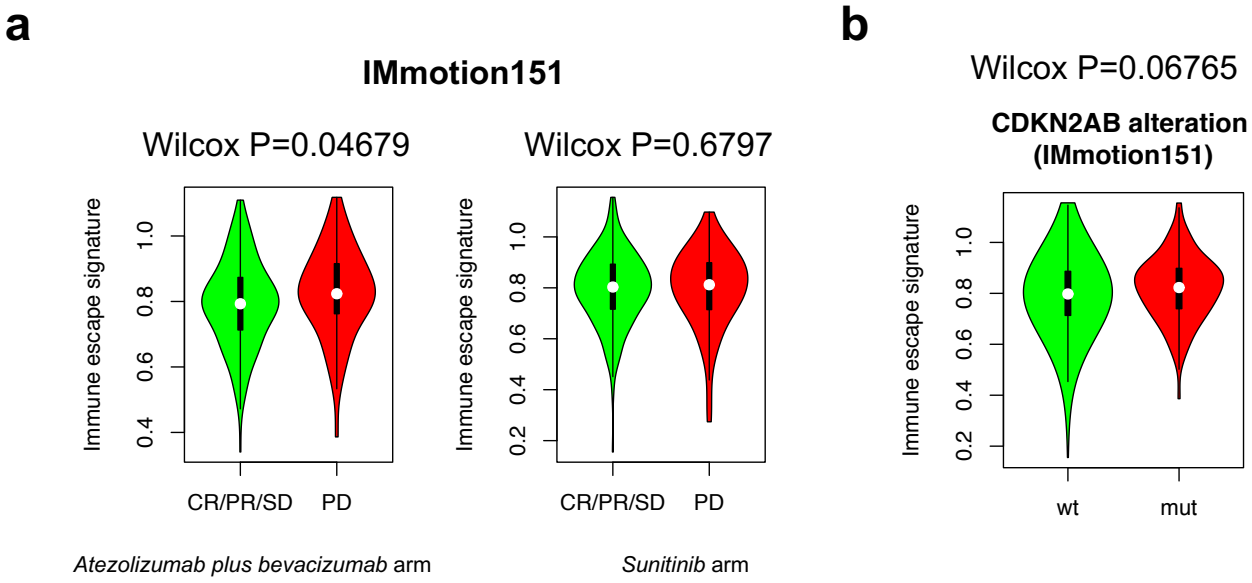

Extended Data Fig. 10

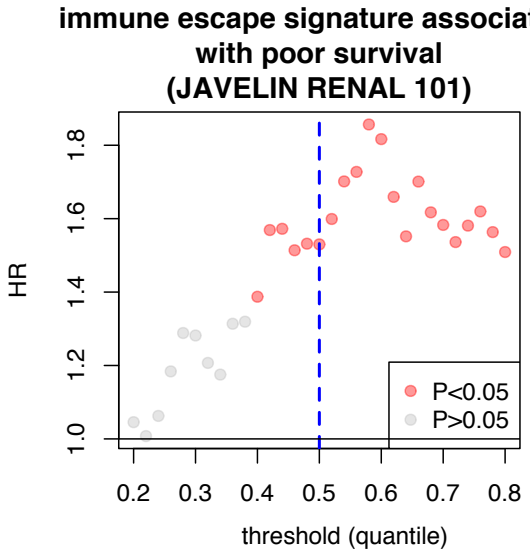

RJ Motzer *et al.* (JAVELIN Renal 101) n=354

Avelumab plus Axitinib

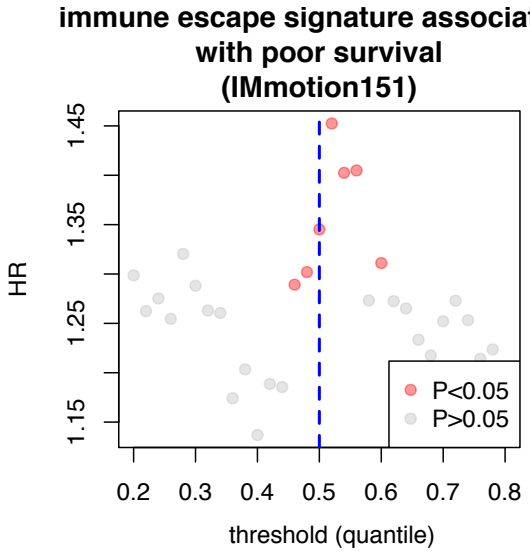

RJ Motzer *et al.* (IMmotion151) n=407

Atezolizumab plus bevacizumab

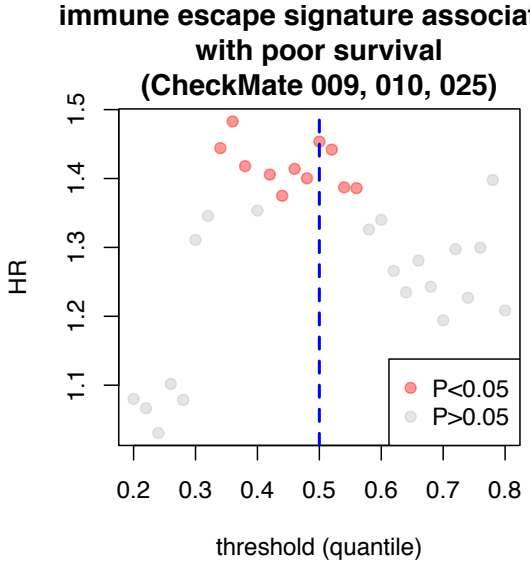

DA Braun *et al.* (CheckMate 009, 010, 025) n=181

Anti-PD1-treatment

Extended Data Fig. 11